Robust USV Control

Active Disturbance Rejection Control for Trajectory Tracking of a Seagoing Unmanned Surface Vessel: Design, Simulation, and Field Experiments

Master's Thesis

Jelmer S. van der Saag

Delft University of Technology

DEMCON | UNMANNED SYSTEMS

TU Delft

AMR Lab

Robust USV Control

Active Disturbance Rejection Control for Trajectory Tracking of a Seagoing Unmanned Surface Vessel: Design, Simulation, and Field Experiments

by

Jelmer S. van der Saag

to obtain the degree of Master of Science
at the Delft University of Technology,
to be defended publicly on February 17th, 2025.

Student Number:	4834259	
Thesis Duration:	August 19, 2024 – February 17th, 2025	
Supervisors:	Dr. J. Alonso-Mora,	TU Delft, Department Supervisor.
	ir. E. Trevisan,	TU Delft, Daily Supervisor.
	Dr. ir. W. Falkena,	Demcon Unmanned Systems, Company Supervisor.

Cover: Demcon Unmanned Systems V2500 operating at the Zevenhuizerplas, Netherlands. © Demcon Unmanned Systems. Image borders extended and upscaled using AI tools.

DEMCON | UNMANNED SYSTEMS TU Delft AMR Lab

Preface

Completing this thesis at Demcon Unmanned Systems has been the most enriching experience of my academic career. The opportunity to work in a commercial setting, collaborate with talented and experienced engineers, and see my work realised during field tests has been profoundly informative.

I extend my deepest gratitude to Demcon Unmanned Systems for their generosity in supporting my research over the past year. Their willingness to allocate time, effort, and resources enabled me to conduct field trials that would have been exceedingly difficult within a purely academic setting. I sincerely thank the entire team for their invaluable assistance, whether in answering technical questions or providing support during testing—both physically and mentally.

In particular, I am immensely grateful to my company supervisor, Dr. ir. Wouter Falkena. His guidance on the various systems and software that I encountered during my time at Demcon Unmanned Systems was invaluable. His reasoned and practical perspective helped refine my ideas and theories, ultimately leading to a more nuanced and well-founded conclusion.

I also wish to express my sincere appreciation to ir. Elia Trevisan, my daily supervisor throughout this process. His patience in addressing my numerous questions on best practices and our control theory discussions provided me with a level of understanding that I would likely not have arrived at on my own. Moreover, his endurance in reviewing the many pages of drafts I sent him has helped enormously in putting this work to paper. His keen insight has had a profoundly positive impact on this entire process. I extend my gratitude as well to my department supervisor, Dr. Javier Alonso-Mora, whose involvement in the TRiLOGy project laid the foundation for both my internship and this thesis, enabling my position at Demcon Unmanned Systems and my work here over the past year.

Finally, I am deeply thankful for the unwavering support of my friends and family. Their encouragement through the inevitable ups and downs of this journey has been invaluable. Their presence and support during demanding times have been a source of strength and motivation, and for that, I am truly grateful.

Jelmer S. van der Saag
Delft, February 2025

Abstract

Unmanned Surface Vessels (USVs) face significant control challenges due to uncertain environmental disturbances, such as waves and currents. This thesis proposes a trajectory tracking controller based on Active Disturbance Rejection Control (ADRC) implemented on the DUS V2500, a seagoing USV developed by Demcon Unmanned Systems. A custom simulation incorporating realistic wave, wind, and current disturbances is developed to validate the performance of the controller. Simulated experiments are supported by further validation through field tests in the harbour of Scheveningen, the Netherlands, and at sea. Simulation results demonstrate that ADRC significantly reduces cross-track error across all tested conditions compared to a baseline PID controller, but increases control effort and energy consumption. Field trials in Scheveningen, the Netherlands, confirm a reduction in cross-track error, while revealing a further increase in energy consumption during sea trials compared to the baseline controller. Modifications to the controller are proposed to improve its efficiency, and the impacts on tracking performance are discussed.

Contents

Nomenclature

Abbreviations

ADRC	Active Disturbance Rejection Control
DOF	Degrees-of-Freedom
DUS	Demcon Unmanned Systems
DWP2	Dynamic Water Physics 2
ESO	Extended State Observer
GNSS	Global Navigation Satelite System
IMU	Inertial Measurement Unit
LOS	Line-of-Sight
MAD	Mean Absolute Deviation
MIMO	Multi-Input Multi-Output
MPC	Model Predictive Control
NED	North-East-Down
NLSEF	Nonlinear Error State Feedback
PID	Proportional-Integral-Derivative
RMS	Root Mean Square
RMSE	Root Mean Square Error
RPM	Rotations Per Minute
RTF	Real-Time Factor
SISO	Single-Input Single-Output
SITL	Software-In-The-Loop
SMC	Sliding Mode Control
TD	Tracking Differentiator
USV	Unmanned Surface Vessel
XTE	Cross-Track Error

Symbols

Symbol	Definition	Unit
b_0	ADRC control scaling coefficient	[-]
c	ADRC damping factor parameter	[-]
e_i	$(i-1)$th derivative of state error e	[-]
$F(t)$, z_3	ADRC "total disturbance"	[-]
h	ADRC filter factor parameter	[-]
r	ADRC tracking speed parameter	[-]
v	Controller setpoint	[-]
v_i	$(i-1)$th derivative of setpoint transient profile	[-]
x_i	$(i-1)$th derivative of system state x	[-]
y	System output	[-]
z_i	$(i-1)$th derivative of state estimation z	[-]
$\mathbf{w}(t) \in \mathbb{R}^3$	External disturbances	[N]
$\boldsymbol{B} \in \mathbb{R}^{3\times3}$	Actuator configuration matrix	[-]
$\boldsymbol{C}(\boldsymbol{\nu}) \in \mathbb{R}^{3\times3}$	Coriolis and centripetal force matrix	[-]
$\boldsymbol{D}(\boldsymbol{\nu}) \in \mathbb{R}^{3\times3}$	Damping matrix	[-]
$\boldsymbol{M} \in \mathbb{R}^{3\times3}$	Rigid-body and added mass inertia matrix	[-]
$\boldsymbol{R}(\psi) \in \mathbb{R}^{3\times3}$	Rotation matrix	[-]
β	State observer gain	[-]
γ	ADRC disturbance rejection scaling coefficient	[-]
Ω	Thruster speed	[rpm]
ψ	Heading	[rad]
τ_d	Time constant for first-order system	[s]
$\boldsymbol{\eta} \in \mathbb{R}^3$	Position and rotation vector	[m] / [rad]
$\boldsymbol{\nu} \in \mathbb{R}^3$	Velocity and rotational speed vector	[m s^{-1}] / [rad s^{-1}]
$\boldsymbol{\tau} \in \mathbb{R}^3$	Control output vector	[N]

1 Introduction

This chapter introduces the thesis, outlining its background, research objectives, and contributions. Section 1.1 presents the background and motivation for selecting this research topic, highlighting its relevance and importance. A review of related literature is provided in Section 1.2, focusing on developments in Active Disturbance Rejection Control (ADRC) and Unmanned Surface Vessel (USV) trajectory tracking in general. The research objectives and main contributions of this work are detailed in Section 1.3. Finally, an overview of the thesis structure is presented in Section 1.4.

1.1. Background and Motivation

While two-thirds of the Earth's surface is covered by oceans and approximately 37% of the global population resides within 100 kilometres of a shoreline [1], the ocean floor remains largely unmapped, with only 15% coverage as of July 2019 [2]. The maritime domain, although still largely unexplored, remains critical for economic, scientific and military advancements [3], underscoring the need for technological developments in maritime exploration and navigation.

One such development has been the introduction of the Unmanned Surface Vessel (USV). These semi-autonomous vessels typically forgo an on-board crew, relying instead on a remote human operator or no operator at all. This shift significantly reduces crew requirements compared to traditional crewed vessels, resulting in lower operational costs and improved work safety, as an operator can remain in a safe environment [3]. Furthermore, the absence of a crew enables the design of smaller and more energy efficient vessels, thus reducing their environmental footprint [4]. These benefits make USVs a suitable alternative to conventional vessels for a wide range of applications, including hydrographic surveys, offshore inspections, and maritime exploration [5], [6].

The maritime environment in which USVs operate poses significant challenges due to environmental factors such as waves, currents, and wind. These disturbances are often unpredictable and negatively impact tasks such as trajectory tracking. In particular, waves, which exist as a spectrum of individual frequencies and incoming directions, are difficult to predict, as the exact wave spectrum must be defined to determine the wave loads on the vessel [7]. Since waves are often generated by distant winds from multiple directions, accurately predicting them is challenging and requires additional sensors to estimate the wave spectrum [8]. An overview of such a wave spectrum and its causes is shown in Figure 1.1.

The control problem for USV path-following under such disturbances has been approached in a variety of ways, including optimal control techniques such as Model Predictive Control (MPC), adaptive methods like backstepping control, and neural networks for control law design [9]. The wide range of design approaches highlights a lack of consensus on an ideal strategy for USV control, presenting an opportunity to investigate less conventional control techniques.

While Proportional-Integral-Derivative (PID) control remains prevalent in USV path-following control due to its simplicity and minimal reliance on system models [9], alternative approaches such as Sliding Mode Control (SMC) [10], feedback linearisation [11], and backstepping control [12] are also common

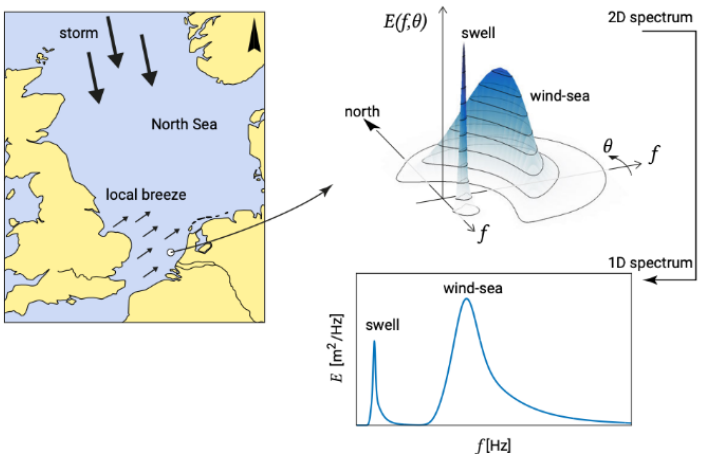

Figure 1.1: Wave frequency spectrum off the Dutch coast, showing the combined effect of swell, generated by distant storms, and local wind waves. Note that the energy of the swell waves is higher in the 2D spectrum, whereas the local wind peak is larger in the 1D spectrum due to greater directional spreading [7].

Figure 1.2: DUS V2500 USV platform, operating near-shore in calm conditions in Scheveningen, the Netherlands. © Demcon Unmanned Systems.

techniques for USV path-following control. However, these methods often require varying levels of system information, limiting their practicality in uncertain and dynamic maritime environments.

An alternative control strategy that aims to reduce model dependency is ADRC, to which a detailed introduction can be found in Chapter 2. This method has gained traction in USV control due to its ability to estimate system dynamics and external disturbances without requiring explicit system information [13]. Although numerous simulation studies have demonstrated the effectiveness of ADRC in USV control [14]–[19], real-world validation remains scarce. Existing experimental validations are predominantly limited to inland waters [20], which lack significant environmental disturbances such as large waves and strong currents.

This thesis seeks to address this gap by implementing and validating an ADRC-based control strategy on the DUS V2500, a fully electric USV developed by Demcon Unmanned Systems (DUS). This vessel, depicted in Figure 1.2, is capable of operating in conditions up to Sea State 4, making it a suitable platform for evaluating ADRC performance in near-shore environments. The performance of the proposed control strategy will be assessed through a Unity simulation with realistic waves and currents and field trials conducted in Scheveningen, the Netherlands. These trials aim to evaluate the performance and feasibility of ADRC for applications in commercial, seagoing USVs.

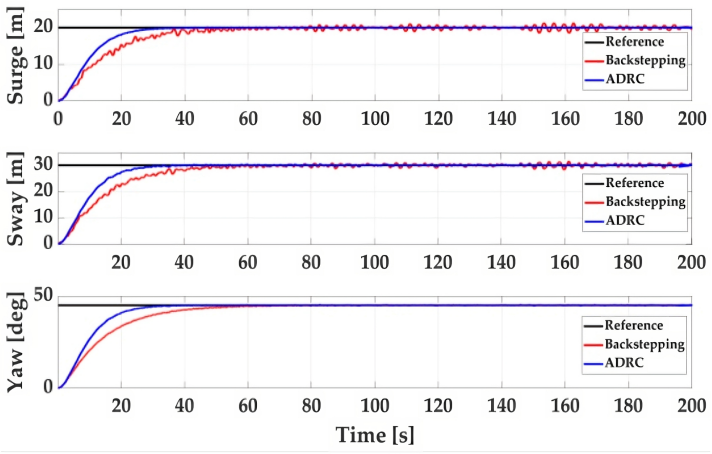

Figure 1.3: Comparison of backstepping control to ADRC for dynamic positioning of a USV in simulation, exposed to both wave and wind disturbances [19].

1.2. Related Works

A comprehensive review of the literature on USV path-following control shows that there is a general lack of studies that evaluate USV control algorithms in real-world conditions [9]. This review, surveying 80 papers published between 2002 and 2022, reveals that approximately 80% of these papers rely primarily on simulations for validation. This reliance on simulation can be attributed to factors such as limited access to appropriate testing facilities and hardware constraints. While novel controller designs are frequently proposed, the absence of field-testing leaves many control strategies untested under real-world conditions. ADRC is an example of such a strategy, having gained popularity in USV control due to its ability to estimate system dynamics and external disturbances without the need for a detailed system model [13], but has seen limited real-world testing for USV control [20].

One of the most frequently cited works on ADRC is [13] and has become the primary reference in discussion on the control strategy. This is partly due to the limited availability of Prof. Han's original work developing ADRC, which is largely only available in Chinese. With over 6000 citations, [13] remains the definitive reference for ADRC, despite the limited access to referenced original material. Several studies have extended the ADRC framework in the context of USV control [14]–[20]. For example, [14] uses a simulated rudder-controlled USV to compare a baseline ADRC controller to an enhanced variant that incorporates the firefly algorithm (FA) for online tuning of ADRC parameters. This modification results in improved simulation performance compared to the baseline approach. The self-tuning aspect of ADRC controllers is further explored in other studies, where techniques such as the use of a fuzzy controller to make adjustments to ADRC parameters [16], particle swarm optimisation [18], and reinforcement learning [17] have been applied to automatically adjust ADRC parameters.

Further extensions of the ADRC framework have involved higher-order state observers and controller topologies. For example, [15] simulated a rudder-controlled USV using a third-order ADRC controller, though no direct comparison with the second-order ADRC controller was made, making it difficult to assess the advantages of this added complexity.

The use of ADRC for dynamic positioning has also been investigated [19]. The study demonstrates the advantages of ADRC over backstepping control in simulation, highlighting its robustness to external disturbances. However, like many studies in this field, this work is limited to simulations. A comparison of the two controllers in simulation can be seen in Figure 1.3.

Despite the numerous studies demonstrating the effectiveness of ADRC in USV control, especially in simulation environments, there remains a significant gap in real-world validation. The only literature available that contains field tests of the ADRC framework in the context of USV control is a study using a custom research vessel, which evaluates a modified ADRC controller [20]. This modified framework integrates a single-layer ELM neural network into the feedback loop with the state observer. The study compares this modified ADRC approach to the baseline ADRC method, as shown in Figure 1.4, but

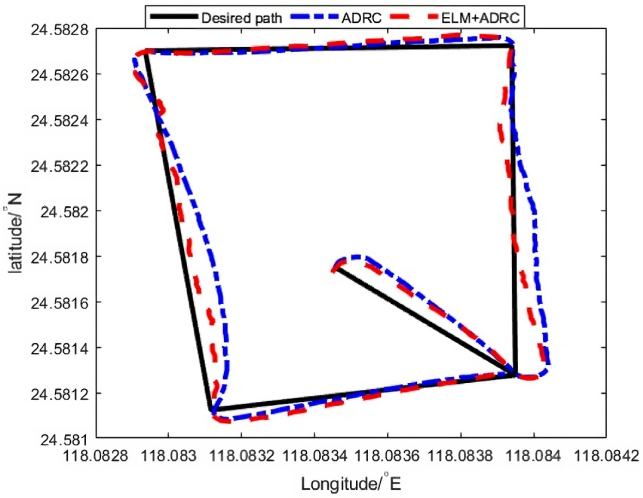

Figure 1.4: Results of field-testing of an ADRC and controller in an inland lake using a custom USV platform [20].

does not provide a direct comparison with more well-established controllers, such as PID. Furthermore, these field tests were conducted in a lake environment, where disturbances from waves and currents are minimal. This raises questions about the performance of such a controller in more challenging environments.

In summary, while numerous studies have demonstrated the effectiveness of ADRC in USV control, particularly in simulation environments, there remains a lack of real-world validation, especially in challenging conditions such as offshore environments. This thesis aims to address this gap by evaluating the performance of ADRC in a real-world maritime setting using the DUS V2500 as an experimental platform.

1.3. Research Objective and Contributions

The objective of this research is to evaluate the performance and feasibility of ADRC as a trajectory tracking control strategy for USVs operating in maritime environments. Using the DUS V2500 as the experimental platform, a second-order ADRC controller is implemented, and its performance is compared with PID under realistic operational conditions. The research focuses on assessing ADRC in terms of tracking accuracy, efficiency, and practical applicability for commercial USVs, compared to a baseline PID controller. This is summarised by the following research question:

Research Question

How does the performance of a second-order Active Disturbance Rejection Control strategy for trajectory tracking compare to a Proportional-Integral-Derivative controller, when evaluated through simulation and field experiments?

The contributions of this thesis are threefold:

- Design and integration of a second-order ADRC controller for trajectory tracking in the on-board control computer of the DUS V2500.
- Development and verification of a Unity-based simulation environment replicating wave, current, and wind disturbances for ADRC validation.
- Validation and comparative analysis of the trajectory-tracking ADRC controller through simulation and real-world experiments, evaluating tracking performance and control effort against a baseline PID controller.

1.4. Thesis Outline

This thesis is centred around a scientific paper in Chapter 2, formatted in the IEEE style and intended for submission to the 2025 International Conference on Intelligent Robots and Systems or other relevant journals and conferences. The paper serves as a standalone document, presenting the thesis' key contributions and results, as well as the necessary preliminaries and background theory to understand the topic. Chapter 3 focuses on the design of the simulation environment used for the experimental work. While briefly addressed in Chapter 2, this chapter delves into additional design aspects and considerations not covered in the paper. Chapter 4 and Chapter 5 provide further results, discussions, and considerations for the simulation experiments and field-testing experiments, respectively. These chapters expand on the findings presented in Chapter 2 and include new results and discussions omitted from the paper for the sake of brevity. The thesis is concluded with Chapter 6.

2

Scientific Paper

This chapter presents a scientific paper as a key outcome of the work conducted during this thesis. Written in the IEEE format, the paper contains the primary contributions of the thesis, results, and background theory. The paper is intended for submission to a relevant journal or conference, such as the 2025 International Conference on Intelligent Robots and Systems.

Active Disturbance Rejection Control (ADRC) for Trajectory Tracking of a Seagoing USV: Design, Simulation, and Field Experiments

Jelmer van der Saag, Elia Trevisan, Wouter Falkena and Javier Alonso-Mora

***Abstract*—Unmanned Surface Vessels (USVs) face significant control challenges due to uncertain environmental disturbances, such as waves and currents. This paper proposes a trajectory tracking controller based on Active Disturbance Rejection Control (ADRC) implemented on the DUS V2500. A custom simulation incorporating realistic wave, wind, and current disturbances is developed to validate the performance of the controller, supported by further validation through field tests in the harbour of Scheveningen, the Netherlands, and at sea. Simulation results demonstrate that ADRC significantly reduces cross-track error across all tested conditions compared to a baseline PID controller, but increases control effort and energy consumption. Field trials in Scheveningen, the Netherlands, confirm a reduction in cross-track error, while revealing a further increase in energy consumption during sea trials compared to the baseline controller.**

***Index Terms*—Unmanned Surface Vessel, Active Disturbance Rejection Control, Robust Control, Trajectory Tracking, Field Experiments.**

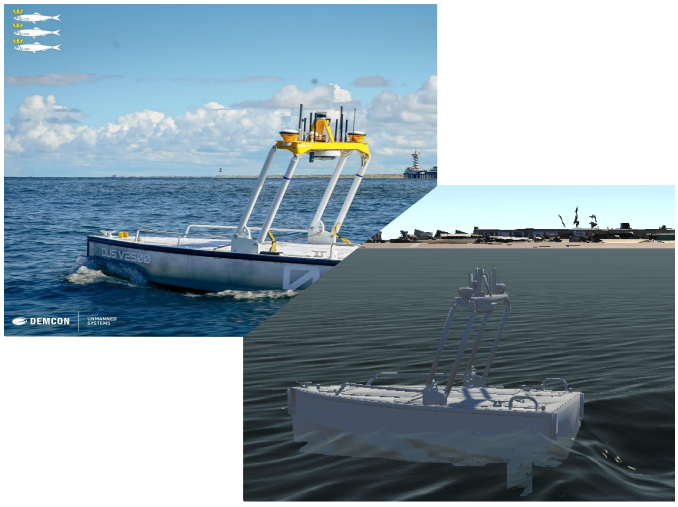

Fig. 1. DUS V2500 USV platform, operating near-shore in calm conditions in Scheveningen, the Netherlands (left) © Demcon Unmanned Systems. and in similar conditions in simulation (right).

I. Introduction

WHILE two-thirds of the Earth's surface is covered by oceans and approximately 37% of the global population resides within 100 kilometres of a shoreline [1], the ocean floor remains largely unmapped with only 15% coverage as of July 2019 [2]. The maritime domain, although still largely unexplored, remains critical for economic, scientific and military advancements [3], underscoring the need for technological developments in maritime exploration and navigation.

One such development has been the introduction of the Unmanned Surface Vessel (USV). These semi-autonomous vessels typically forgo an on-board crew, relying instead on a remote human operator or no operator at all. This shift significantly reduces crew requirements compared to traditional crewed vessels, resulting in lower operational costs and improved work safety, as an operator can remain in a safe environment [3]. Furthermore, the absence of a crew enables the design of smaller and more energy efficient vessels, thus reducing their environmental footprint [4]. These benefits make USVs a suitable alternative to conventional vessels for a wide range of applications, including hydrographic surveys, offshore inspections, and maritime exploration [5], [6].

The maritime environment in which USVs operate can be particularly challenging due to the impact of environmental factors such as waves, currents, and wind. These disturbances are often unpredictable and negatively impact tasks such as trajectory tracking. Despite these challenges, path-following control for USVs has often relied on traditional control methods. For path-following control of USVs, Proportional-Integral-Derivative (PID) control remains the primary control method, for its simplicity and ability to provide satisfactory performance under most conditions [7]. However, PID control may struggle to maintain performance in the presence of nonlinear system dynamics or rapidly changing environmental disturbances, leading to reduced performance in more challenging environments.

In recent years, various control strategies have been proposed to improve USV performance in dynamic environments. While PID control remains dominant due to its simplicity and minimal reliance on system models, alternatives such as Sliding Mode Control (SMC) [8], feedback linearisation [9], and backstepping control [10] have been widely applied [7]. However, these methods require varying levels of system information, limiting their practicality in uncertain maritime conditions. Recent advances, such as the use of neural networks to approximate unknown model dynamics [11] and techniques to replace system information with rapid measurements of state and disturbance estimation [12], have aimed to reduce this dependency.

One such technique aiming to eliminate model dependency is Active Disturbance Rejection Control (ADRC), which has seen adoption in the field of USV control due to its ability to

estimate uncertain system dynamics and external disturbances without any system information [13]. The method allows for estimation of the "total disturbance" acting on the system, including both internal uncertainties and external disturbances, which is then compensated via a feed-forward component.

Although the effectiveness of ADRC in USV control has been repeatedly demonstrated in simulation studies [14]–[19], real-world validations are limited. Existing experiments have been conducted only in inland waters [20] which lack significant disturbances such as stronger waves and currents. To the best of the authors' knowledge, no prior research has evaluated the performance of ADRC implemented on a seagoing USV through real-world testing.

This study addresses this gap by designing and validating an ADRC-based control strategy on the DUS V2500, a fully electric USV developed by Demcon Unmanned Systems (DUS) as shown in Fig. 1. Capable of operating in conditions up to Sea State 4, the DUS V2500 serves as a suitable platform for evaluating ADRC performance in near-shore conditions. Performance will be evaluated through simulation in a Unity environment, featuring realistic waves and currents, and field trials in Scheveningen, The Netherlands. Through these tests, we aim to evaluate the feasibility of ADRC for seagoing applications. The contributions of this paper are therefore as follows:

- The design and implementation of a trajectory-tracking second-order ADRC controller for the DUS V2500.
- Development and verification of a Unity-based simulation environment replicating wave, current, and wind disturbances for ADRC validation.
- Validation and comparative analysis of the ADRC controller through simulation and real-world experiments, evaluating tracking performance and control effort against a baseline PID controller.

II. Preliminaries

This section provides an overview of the DUS V2500 platform, followed by a description of the system dynamics. The section concludes with an overview of the actuator dynamics.

A. USV Platform

The DUS V2500, as shown in Fig. 1, is a fully electric USV designed by Demcon Unmanned Systems for applications such as inspection and hydrography. The vessel measures approximately 2.5 metres in length and is primarily intended for inland and near-shore operations. It is rated to operate in conditions up to Douglas Sea State 4, corresponding to wave heights of up to 2.5 metres.

The platform is underactuated, featuring two stern-mounted thrusters and a single bow thruster for manoeuvring. The DUS V2500 operates without an on-board crew and is semi-autonomous, executing missions autonomously based on a predefined global mission plan that is configured and monitored by a remote operator.

The vessel's localisation is achieved through the fusion of Global Navigation Satelite System (GNSS) and Inertial Measurement Unit (IMU) data, providing accurate estimates of the pose, velocity, and acceleration of the vessel for control purposes. A detailed description of the system architecture of the DUS V2500 is beyond the scope of this paper, and remains proprietary to Demcon Unmanned Systems.

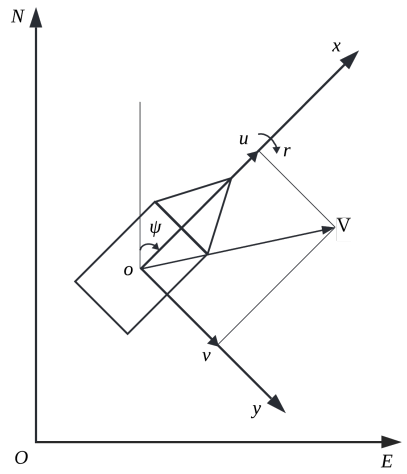

Fig. 2. Planar manoeuvring diagram of a USV where NOE denotes the geodetic NED coordinate system with O as the origin, and xoy denotes the body-fixed coordinate system with o as the USV's centre of gravity. V is the resulting velocity vector of u and v.

B. System Dynamics

The dynamics of a ship are typically described in six degrees-of-freedom (DOF), where (x, y, z) represent the vessel's position in three-dimensional space, and (ϕ, θ, ψ) denote its orientation. However, for manoeuvring models, it is commonly assumed that the ship is laterally and longitudinally stable, with $\phi = \theta = \dot{\phi} = \dot{\theta} \approx 0$ [21]. In addition, the ship is assumed to float, with a mean value of $z \approx 0$.

Under these assumptions, the model can be reduced to a 3-DOF system described by $\eta = [x, y, \psi]^\intercal$ and $\nu = [u, v, r]^\intercal$, where (x, y) represents the Cartesian position in the geodetic North-East-Down (NED) reference frame, ψ is the yaw angle, (u, v) are the body-fixed velocities (referred to as surge and sway), and r is the yaw rate. The resulting system has a workspace of $\mathbb{R}^2$ and a configuration space of $\mathbb{R}^2 \cdot \mathbb{S}^1$. A diagram of the manoeuvring model is provided in Fig. 2.

The system dynamics are defined by the following equations [21]:

$$\begin{cases} \dot{\eta} = \mathbf{R}(\psi)\nu \\ \dot{\nu} = \mathbf{M}^{-1}\big(-\mathbf{C}(\nu)\nu - \mathbf{D}(\nu)\nu + \tau + \mathbf{w}(t)\big) \end{cases} \tag{1}$$

where $\mathbf{R}(\psi)$ is the rotation matrix:

$$\mathbf{R}(\psi) = \begin{bmatrix} \cos\psi & -\sin\psi & 0 \\ \sin\psi & \cos\psi & 0 \\ 0 & 0 & 1 \end{bmatrix}. \tag{2}$$

For this system, $\mathbf{M}$ represents the mass and added mass matrix, $\mathbf{C}(\nu)$ is the Coriolis and centripetal matrix, $\mathbf{D}(\nu)$ is the damping matrix, τ contains the forces and moments generated

by the actuators, and $\mathbf{w}(t)$ denotes external disturbances acting on the system, such as wind or currents.

The matrices $\mathbf{M}$, $\mathbf{C}(\boldsymbol{\nu})$, and $\mathbf{D}(\boldsymbol{\nu})$ contain hydrodynamic coefficients. The specific configurations of these matrices can vary greatly depending on the chosen model, but the system dynamics are generally nonlinear and coupled due to the dependency of $\mathbf{C}(\boldsymbol{\nu})$ and $\mathbf{D}(\boldsymbol{\nu})$ on the velocity vector $\boldsymbol{\nu}$ [21], [22].

The accuracy of such a model is highly dependent on the correct identification of these coefficients. Although the sensitivity of the model to each coefficient varies, a small discrepancy in one of the more sensitive parameters can lead to significant deviations in the model's output [23].

Modelling disturbances $\mathbf{w}(t)$, including currents, waves, and wind, presents additional challenges. Accurate estimation of these effects during operation requires sensors to measure free-stream air and water velocity, or additional sensors for radar-based techniques to estimate the wave spectrum [24]. These sensors are currently not present on the DUS V2500 platform, limiting its ability to predict environmental disturbances.

C. Actuator Dynamics

Since the vessel is rudderless, the control input vector τ is defined as [21]:

$$\tau = \mathbf{B}\mathbf{f}_{\mathbf{c}}(\boldsymbol{\nu}, \mathbf{n}) \tag{3}$$

where $\mathbf{B} \in \mathbb{R}^{3\times3}$ represents the actuator configuration matrix, and $\mathbf{f}_{\mathbf{c}}(\boldsymbol{\nu}, \mathbf{n}) \in \mathbb{R}^3$ is a function that outputs the vector of forces and moments as a function of body-fixed velocity $\boldsymbol{\nu}$ and actuator setpoints $\mathbf{n}$.

For the DUS V2500, a thrust curve that relates the rotational speed of the thrusters to the produced thrust is available. However, this relationship does not account for the fluid velocity entering the thrusters, leaving $\mathbf{f}_{\mathbf{c}}(\boldsymbol{\nu}, \mathbf{n})$ effectively unknown. As a result, it is challenging to accurately estimate the forces produced by each thruster.

Furthermore, the rotational speed of the thruster cannot be changed instantaneously, due to spin-up and spin-down delay caused by rotational inertia and propeller drag. However, this delay can be approximated as a first-order low-pass filter [25]. In the Laplace domain, this is expressed as:

$$\Omega(s) = \frac{\Omega_0(s)}{1 + s\tau_d} \tag{4}$$

where $\Omega(s)$ denotes the actual thruster speed, $\Omega_0(s)$ is the thruster setpoint, and τ_d represents the time constant of the system. For a first-order system, the time constant can be approximated as $\tau_d = T_s/4$, where T_s is the settling time of the system [26].

For the DUS V2500, the settling times were identified as approximately $T_s \approx 2$ seconds for the stern thrusters and $T_s \approx 1$ second for the bow thruster. These values correspond to time constants of $\tau_d = 0.5$ seconds and $\tau_d = 0.25$ seconds, respectively. This approximation is compared to the thrust data measured from the vessel in Fig. 3. Although it should be noted that this is not a precise approximation, ADRC is not reliant on an accurate model of the plant, and such a linear approximation has previously demonstrated success in delay compensation [13], [25].

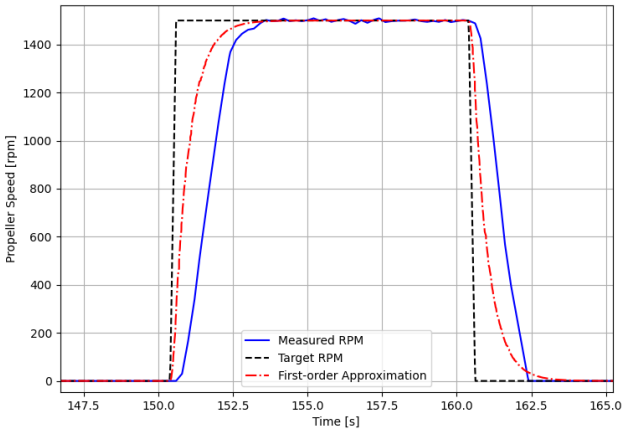

Fig. 3. First-order approximation compared to measured thrust data from a stern thruster of the DUS V2500.

III. Active Disturbance Rejection Control

This section first introduces the primary design principle behind ADRC, followed by an overview of a typical ADRC scheme and its basic components.

A. ADRC Design Principle

As outlined in Sec. II, accurately modelling either the system or the disturbances acting on it is a significant challenge. In seagoing USVs, which are subject to considerable and often unpredictable disturbances, this limitation restricts the applicability of model-based control techniques. In contrast, ADRC reframes the problem by eliminating the need for precise knowledge of the system dynamics or disturbances. Instead, the unknown dynamics and external disturbances are seen as something to overcome by the control signal [13].

Consider a second-order system represented by the following equations:

$$\begin{cases} \dot{x_1} = x_2 \\ \dot{x_2} = F(t) + bu \\ y = x_1 \end{cases} \tag{5}$$

where y is the system output, u represents the input and $F(t) = f(x_1, x_2, w(t), t)$ describes both the system states x_1 and x_2, and disturbances $w(t)$ as a function of time. Although $F(t)$ may be unknown, it can still be compensated for by adjusting the control effort u to regulate the system output. In ADRC, $F(t)$ is treated as an additional state variable, termed the "total disturbance" and denoted as x_3. This reformulates the original system as:

$$\begin{cases} \dot{x_1} = x_2 \\ \dot{x_2} = x_3 + bu \\ \dot{x_3} = G(t) \\ y = x_1 \end{cases} \tag{6}$$

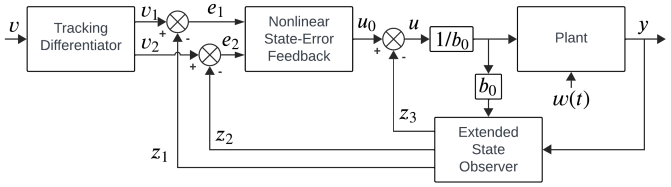

Fig. 4. Standard ADRC topology.

where $G(t) = \dot{F}(t)$. The system can be represented in state-space form as:

$$\begin{cases} \dot{\mathbf{x}} = \begin{bmatrix} 0 & 1 & 0 \\ 0 & 0 & 1 \\ 0 & 0 & 0 \end{bmatrix} \mathbf{x} + \begin{bmatrix} 0 \\ 1 \\ 0 \end{bmatrix} u + \begin{bmatrix} 0 \\ 0 \\ 1 \end{bmatrix} G(t) \\ y = \begin{bmatrix} 1 & 0 & 0 \end{bmatrix} \mathbf{x} \end{cases} \tag{7}$$

From this formulation, it follows that the system is observable, as the observability matrix is of full rank:

$$\mathcal{O} = \begin{bmatrix} \mathbf{C} \\ \mathbf{CA} \\ \mathbf{CA}^2 \end{bmatrix} = \mathbf{I}_3 \tag{8}$$

B. Basic ADRC Scheme

The standard ADRC scheme, as proposed by [13], comprises three primary components. These components are illustrated in Fig. 4 and are described in detail in the following subsection.

1) Extended State Observer: As demonstrated by Eq. 7, the reformulated system is fully observable, enabling the construction of a state observer to estimate the total disturbance x_3. This observer, referred to as the Extended State Observer (ESO), is expressed as:

$$\begin{cases} e = z_1 - y \\ \dot{z_1} = z_2 - \beta_{01} e \\ \dot{z_2} = z_3 + b_0 u - \beta_{02}\,\mathrm{fal}(e, \alpha_1, \delta) \\ \dot{z_3} = -\beta_{03}\,\mathrm{fal}(e, \alpha_2, \delta) \end{cases} \tag{9}$$

where $\mathbf{z}$ is the state observer's estimate of $\mathbf{x}$, β_{01}, β_{02}, and β_{03} are the observer gains, and $\mathrm{fal}(e, \alpha, \delta)$ is a nonlinear function that replaces the proportional error e for z_2 and z_3 [13]. The function $\mathrm{fal}(e, \alpha, \delta)$ is defined as:

$$\mathrm{fal}(e, \alpha, \delta) = \begin{cases} \frac{e}{\delta^{\alpha-1}}, & |e| \le \delta \\ |e|^{\alpha}\,\mathrm{sign}(e), & |e| > \delta \end{cases} \tag{10}$$

Here, δ primarily determines the size of the linear region near the origin, while α controls the slope of the linear region and the slope of the nonlinear region for $|e| > \delta$. This nonlinear function is designed to improve convergence to the system state and while minimising peaking, where the state estimation error temporarily exhibits large transients due to high observer gains, in response to sudden changes or disturbances [27]. The values of α are typically set as $\alpha_1 = 0.5$ and $\alpha_2 = 0.25$ [13]–[15], with δ remaining a user-defined parameter.

As with a standard Luenberger observer, the observer is generally designed to respond significantly faster than the system, with a common guideline being a response time approximately 10 times faster than that of the system [26]. As described in [13], the ESO gains are designed based on the system's speed and are defined as functions of the sampling time h, showing satisfactory performance in simulations across a wide range of values of h.

$$\beta_{01} = 1 \quad \beta_{02} = \tfrac{1}{2h^{0.5}} \quad \beta_{03} = \tfrac{2}{5^2 h^{1.2}} \tag{11}$$

However, currently there is no formal method to determine the optimal gains for the ESO [27]. Instead, these observer gains are often a user-defined parameter, depending on the system. Excessively high gains amplify the noise present in the input signals, which may degrade observer performance [28]. Therefore, gains should be selected for an appropriate balance between convergence speed and noise tolerance.

2) Tracking Differentiator: The Tracking Differentiator (TD) generates a transient profile that the system can reasonably follow, to avoid sudden setpoint jumps. As the ADRC scheme assumes an underlying second-order system, a double integral plant can be used to construct this profile. A discrete-time solution to such a double integral plant is proposed by [13] as:

$$\begin{cases} v_1 = v_1 + h v_2 \\ v_2 = v_2 + h u, & |u| \le r \\ u = \mathrm{fhan}(v_1 - v, v_2, r_0, h_0) \end{cases} \tag{12}$$

Where v_1 and v_2 are the transient state and state derivative, respectively, v is the controller setpoint, r is a parameter that can speed up or slow down the transient profile, and r_0 and h_0 are controller parameters. The discrete time-optimal solution $\mathrm{fhan}(v_1, v_2, r_0, h_0)$ can be written as:

$$\begin{cases} d = r_0 h_0 \\ d_0 = h_0 d \\ y = v_1 + h_0 v_2 \\ a_0 = \sqrt{d^2 + 8r|y|} \\ a = \begin{cases} v_2 + \frac{a_0 - d}{2}\,\mathrm{sign}(y), & |y| > d_0 \\ v_2 + \frac{y}{h}, & |y| \le d_0 \end{cases} \\ \mathrm{fhan} = -\begin{cases} r\,\mathrm{sign}(a), & |a| > d \\ r\frac{a}{d}, & |a| \le d \end{cases} \end{cases} \tag{13}$$

Per [13], this solution guarantees optimal convergence from v_1 to v without overshoot when $r_0 = r$ and $h_0 = h$. However, these parameters may be individually adjusted to change the tracking speed and smoothness of the transient profile, respectively.

3) Nonlinear State Error Feedback: Similar to the TD, the basic ADRC scheme proposes the use of the optimal solution to the double-integral plant, $\mathrm{fhan}(e_1, ce_2, r_1, h_1)$, as a control law [13]:

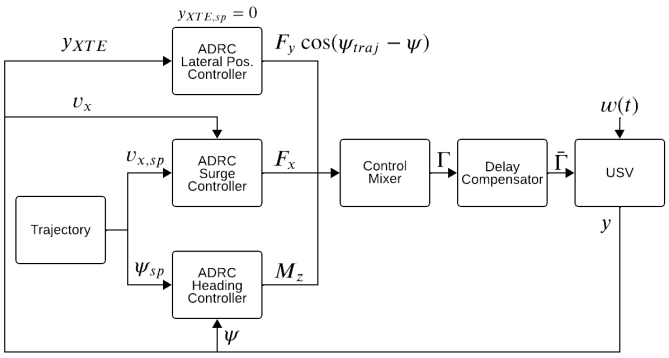

Fig. 5. Design of the trajectory-tracking controller using ADRC topology.

$$\begin{cases} e_1 = v_1 - z_1 \\ e_2 = v_2 - z_2 \\ u_0 = \text{fhan}(e_1, ce_2, r_1, h_1) \\ u = -\frac{u_0 + z_3}{b_0} \end{cases} \tag{14}$$

Where c denotes the damping factor, an additional user parameter, and b_0 represents the control coefficient, which scales the magnitude of the control signal. This control law assumes that the underlying plant is a second-order system, as presented in Eq. 6, with the total disturbance z_3 compensated for via a feed-forward term. Although the ADRC framework can be adapted to incorporate alternative control laws depending on the specific application [13], the use of $\text{fhan}(e_1, ce_2, r_1, h_1)$ is well-suited for USV control. This is due to the similarity between the system dynamics formulated in Eq. 1 and the assumed dynamics of the ADRC controller, as outlined in Eq. 5.

IV. Controller Design

The trajectory controller consists of three ADRC controllers operating in series, as shown in Fig. 5, one for each degree of freedom. Each ADRC controller has a topology identical to that shown in Fig. 4. Although the dynamics of each degree of freedom are coupled, the effective decoupling performance of ADRC allows for individual control of each degree of freedom [19], [29].

The heading setpoint is derived from the trajectory using an L1 guidance law, which steers the USV towards the reference trajectory. The surge velocity is also derived from the trajectory and is set to the mission speed of 1.4m/s, automatically reducing during cornering to improve manoeuvrability. The setpoint of the lateral offset is fixed at zero, ensuring that the vessel follows the trajectory line. The output F_y of the ADRC lateral position controller is projected using the vessel's heading ψ and the trajectory line heading ψ_{traj}, ensuring F_y, and by extension F_B, primarily act when the USV is aligned with the reference trajectory.

A. Control Mixer

The control mixer translates the force and moment demands from the controllers into individual thruster commands. As the system is underactuated, multiple solutions exist; however, under the following assumptions, a unique solution can be derived:

- The bow thruster is used exclusively to control the lateral position of the vessel, with torque being controlled using the stern thrusters.
- The stern thrusters, mounted at an inward angle of α, have a negligible lateral force contribution ($\sin\alpha \approx 0$).

These assumptions allow the control mixer to be defined as:

$$\begin{cases} F_{SL} = \frac{1}{2\cos\alpha}\left(F_x + \frac{M_z + F_y x_{BT}}{y_{ST}}\right) \\ F_{SR} = \frac{1}{2\cos\alpha}\left(F_x - \frac{M_z + F_y x_{BT}}{y_{ST}}\right) \\ F_B = F_y \end{cases} \tag{15}$$

where F_{SL}, F_{SR}, and F_B represent the thrusts of the left stern thruster, right stern thruster, and bow thruster, respectively. The parameters x_{BT} and y_{ST} are geometric dimensions of the USV, denoting the longitudinal distance from the centre of mass to the bow thruster and the lateral distance to the stern thrusters, respectively.

B. Delay Compensator

The delay compensator leverages the first-order approximation of the motor delay, as shown in Fig. 3. For the total control signal $\mathbf{\Gamma} = [F_{SL}, F_{SR}, F_B]^\intercal$, the delay is compensated using the following first-order approximation:

$$\bar{\mathbf{\Gamma}} = \mathbf{\Gamma} + \boldsymbol{\tau}_\mathbf{d}\dot{\mathbf{\Gamma}}, \tag{16}$$

where $\bar{\mathbf{\Gamma}}$ represents the compensated control signal, $\dot{\mathbf{\Gamma}}$ is the derivative of the control signal, and $\boldsymbol{\tau}_\mathbf{d} = [0.5, 0.5, 0.25]^\intercal$ contains the time constants for the stern and bow thrusters.

The derivative $\dot{\mathbf{\Gamma}}$ is calculated using a separate Tracking Differentiator (TD) for each control signal. By setting a large value for r_0, the transient profile of the TD instantly adapts to changes in the input signal, effectively acting as a differentiation filter. This approach offers advantages over numerical differentiation methods, such as improved noise tolerance [30].

V. Simulation

This section outlines the contributions made to a realistic Unity-based maritime simulation framework. An overview of the design of the simulated experiment is then provided, followed by the presentation of the experimental results and a subsequent discussion.

A. Simulation Design

A Software-In-The-Loop (SITL) simulation is used to validate the controller, comprising a digital twin of the on-board control computer, integrated with a Unity-based simulation of vessel dynamics and sensor inputs. This simulation architecture, shown in Fig. 6, provides an environment for validating and evaluating controller performance under realistic operating conditions. An example of a USV in this simulation environment can be seen in Fig. 1 and Fig. 7.

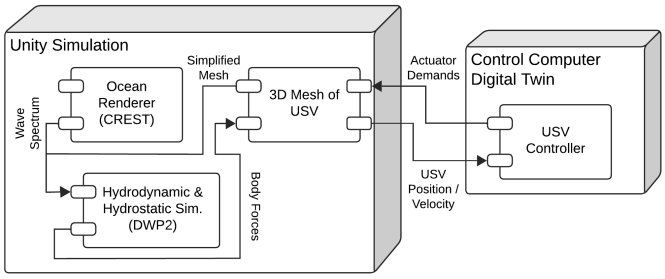

Fig. 6. Architecture of Unity Simulation.

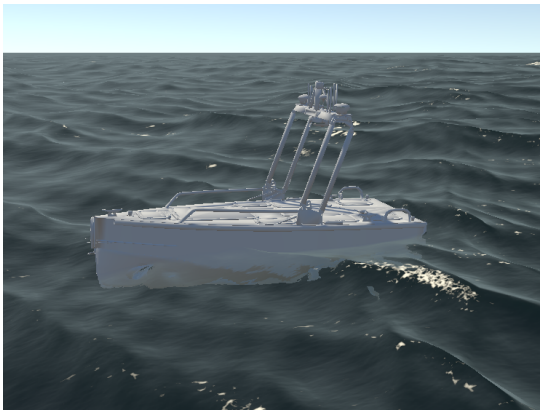

Fig. 7. Unity simulation of the DUS V2500 operating in sea state 4.

This Unity simulation uses the Dynamic Water Physics 2 (DWP2) package to model vessel dynamics in six DOF. Although a 3DOF manoeuvring model of the V2500 is available, based on system identification data, realistic simulation of environmental disturbances requires the inclusion of roll, pitch, and heave dynamics. The DWP2 physics simulation has been validated against the known manoeuvring model of the DUS V2500, as shown in Appendix A. However, verification of the additional degrees of freedom (roll, pitch, and heave), which are primarily influenced by wave disturbances, is limited due to the absence of relevant system identification data or models. Collecting such data is costly, as it would require wave tank experiments to establish known and precise wave conditions.

To simulate a realistic wave environment, DWP2 is integrated with the open-source CREST 4 ocean renderer, which generates a Pierson-Moskowitz wave spectrum. The desired intensity of the wave spectrum can be easily specified to determine the total wave height, with sea states corresponding to Douglas Sea States 1-4 implemented within the simulation. This corresponds to a maximum wave height of 2.5m at sea state 4. Furthermore, CREST 4 supports fluid flow modelling, allowing the inclusion of ocean currents in the simulation.

B. Simulated Experiment Design

A simulated experiment was conducted to evaluate the performance of the ADRC controller against a baseline PID controller in a controlled environment. The experiment used a predefined trajectory within the Derde Haven of Scheveningen,

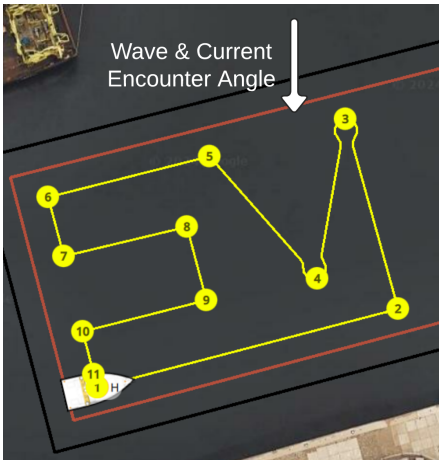

Fig. 8. In-harbour trajectory used for both simulated and real-world tests. The encounter angle for waves and currents applies only to the simulated experiment.

created using the navigation software stack developed by DUS. This software enables waypoint-defined trajectories that are compatible with both simulations and real-world testing.

The simulated experiment trajectory, shown in Fig. 8, consists of a combination of straight paths and corners, including 90-degree and acute turns. Simulated disturbances, including waves and currents, originate from the north, as indicated by the white arrow in the figure. The trajectory is defined with a mission speed of 1.4m/s. To ensure smooth transitions between segments, Dubins curves are employed using a turning radius derived from the mission speed.

Performance of both the ADRC controller and the baseline PID controller – currently deployed on the DUS V2500 – was evaluated using the same trajectory. The PID controller used the gain values implemented in the production vessel, while the gains of the ADRC controller were manually tuned for the experiment. Both controllers followed the control architecture depicted in Fig. 5, with the baseline replacing the ADRC controller with a standard PID controller.

Each controller was assessed in trajectory tracking under four distinct operating conditions:

1) No disturbances,
2) A current of 0.5m/s with no waves,
3) No current with waves at sea state 4 (2.5m wave height),
4) Both a 0.5m/s current and sea state 4 waves.

The performance of the controllers was evaluated based on the following metrics:

Cross-Track Error (XTE): The deviation from the desired trajectory.

Total Battery Usage: The total battery capacity consumed (in Ampere-hours) by the USV, estimated by integrating the current delivered to each motor over the entire trajectory.

C. Results

To evaluate the performance of each controller under varying conditions, five repetitions of the trajectory were conducted for each case to account for error margins. The Root Mean

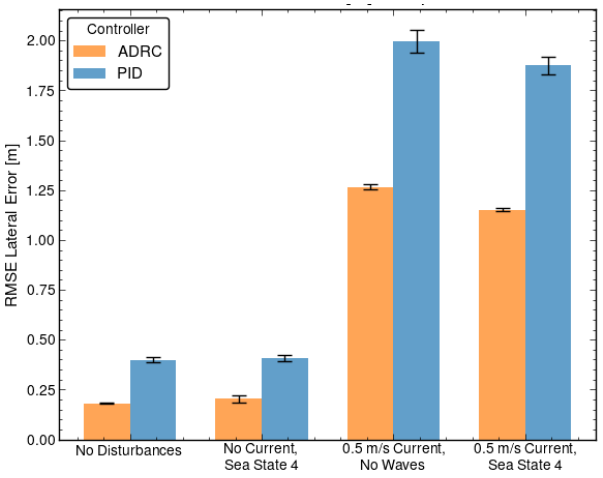

Fig. 9. RMS of the cross-track error (XTE) for each controller, averaged over 5 simulated trajectories. Error bars indicate min- and maximum measured values.

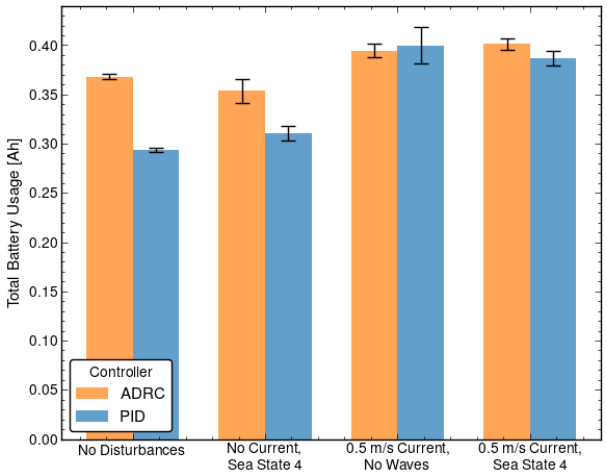

Fig. 10. Total battery consumption of each controller, averaged over 5 simulated trajectories. Error bars indicate min- and maximum measured values.

Square (RMS) of the XTE was computed over the length of each trajectory. This metric for each controller and condition is summarised in Fig. 9. Additionally, the total energy usage for each controller, averaged over 5 trajectories for each testing condition, is presented in Fig. 10.

A sample of the trajectories for both the ADRC and PID controllers, under conditions without disturbances and with all disturbances active (0.5m/s current and sea state 4), is shown in Fig. 11.

D. Discussion

The results show an improvement in performance of the ADRC controller compared to the baseline PID controller across all operating conditions. A noticeable reduction in XTE was observed for both controllers, even in the absence of disturbances. This suggests that the control law implemented in ADRC (see Eq. 14) yields more effective trajectory tracking than the PID control law.

A similar trend was observed in the presence of current, with the ADRC controller demonstrating better performance, likely due to its enhanced control law rather than improved disturbance rejection. As shown in Fig. 11, both controllers exhibit comparable XTE after having settled to an equilibrium position during straight-line tracking, with the USV maintaining a constant lateral offset caused by the current. This offset occurs when the bow thruster reaches its maximum output and cannot fully compensate for the current disturbance. To address this, alternative guidance laws could shift the equilibrium position closer to the trajectory. An example of a trajectory that uses this modified guidance law can be found in Appendix B.

In addition, tracking performance with wave disturbances was similar to those without, suggesting that waves had minimal impact on the lateral error. Although a slight increase in trajectory variability was observed in Fig. 11, it did not significantly affect XTE. In fact, the presence of waves occasionally resulted in a marginally lower XTE, likely due to increased variability, but possibly also due to limitations in the wave model, which may not accurately capture the transfer of momentum from the waves to the vessel. Despite the introduction of waves increasing pitch, roll, and heave motions, these effects did not significantly affect the vessel's manoeuvring performance.

Battery consumption, depicted in Fig. 10, is lower for the PID controller in scenarios without current and approximately equal to the ADRC controller in scenarios with current. In the presence of current, the battery consumption of ADRC is lower because it completes the trajectory faster with fewer deviations, as shown in Fig. 11.

Fig. 12 reveals that the ADRC controller exhibits higher Rotations Per Minute (RPM) peaks, particularly at the first corner, indicating more aggressive trajectory tracking. However, the average RPM of the ADRC controller prior to the corner is consistently higher and more variable compared to the PID controller, even in the absence of disturbances. This also causes the USV to reach the corner sooner under the ADRC corner than the PID controller.

The observed increase in control effort can be attributed in part to the fundamental principle of ADRC. As formulated in Eq. 6, the "total disturbance" $F(t) = f(x_1, x_2, w(t), t)$ is completely counteracted by the control signal u. This forces the system to behave as a second-order system, actively rejecting both external disturbances and internal higher-order effects. Since ADRC cannot differentiate between these internal dynamics and external disturbances, it results in a more aggressive control output.

The control mixer design amplifies noise significantly, as the stern thrusters must generate both surge and torque forces due to the underactuation of the vessel. Consequently, small torque variations result in large stern thruster RPM fluctuations, as shown in Fig. 13. Minor torque fluctuations of the ADRC heading controller are amplified as the stern thrusters work to provide both torque and thrust. Partially delegating torque to the bow thruster could mitigate this, but requires redesigning the control mixer in Eq. 15.

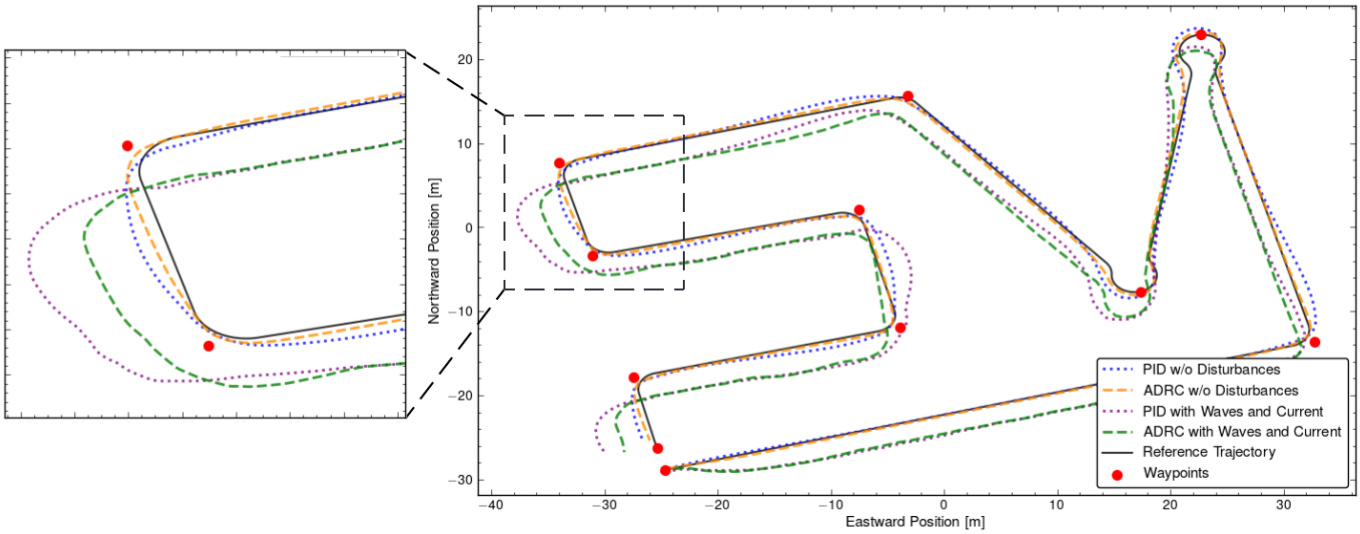

Fig. 11. Comparison of ADRC and PID controllers in simulation under different conditions.

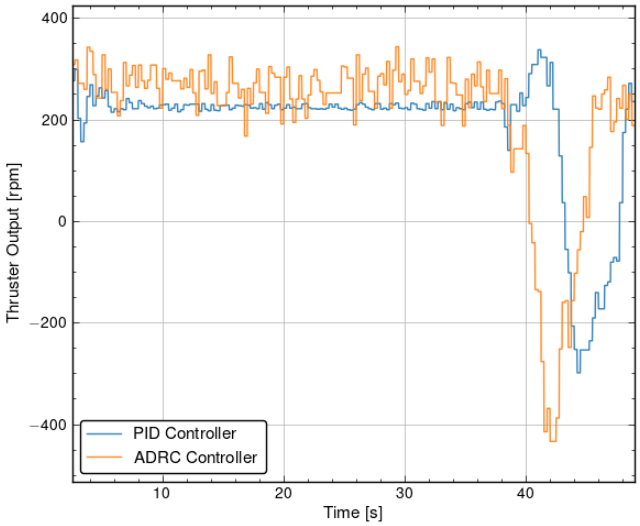

Fig. 12. Comparison of RPM values for a stern thruster during the same simulated trajectory without disturbances.

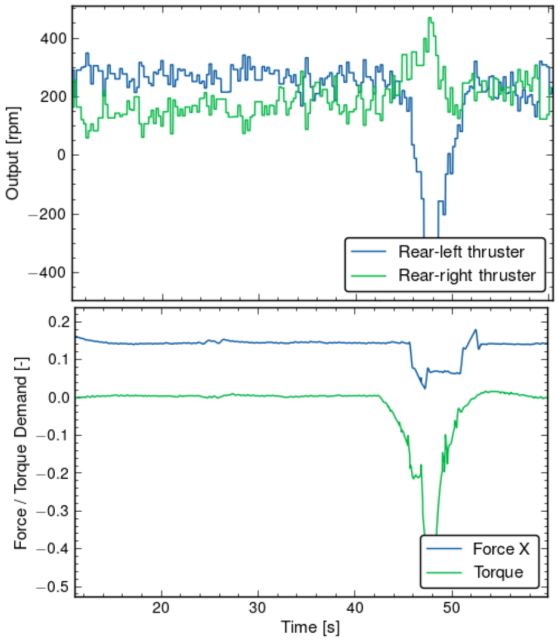

Fig. 13. Comparison of the heading controller's torque output with the stern thruster RPMs after applying the control mixer. Increased noise in the RPM outputs highlights the effects of underactuation and disturbance rejection by the ADRC.

VI. Real-World Testing

Similar to the section on simulated results, this section begins by detailing the design of the field-testing experiments conducted in the harbour of Scheveningen, the Netherlands. An overview of the results is then provided, followed by a comparison to the simulated results and a discussion of their implications.

A. Experiment Design

Field trials were conducted in two scenarios to evaluate the ADRC controller under varying environmental conditions. The first scenario involved replicating a trajectory, defined by the same waypoints as in Fig. 11, within the harbour of Scheveningen. This provided a controlled environment with minimal disturbances, as shown in Fig. 14.

Second, an identical trajectory was tested in a near-shore environment outside the harbour to evaluate performance under increased wave and current disturbances. The trajectory was located approximately 600 metres from the nearest groyne and 1 kilometre from the shore. Fig. 15 provides an on-board view of the DUS V2500 operating in these conditions.

The gains and parameters for both controllers were kept identical to those used in simulation, as they demonstrated satisfactory performance during field tests. This approach ensures a fair comparison between the controllers and highlights

Fig. 14. The DUS V2500 during in-harbour trials in Scheveningen, the Netherlands.

Fig. 15. On-board view of the DUS V2500 during near-shore trials off the coast of Scheveningen, the Netherlands.

their ability to transfer effectively from simulation to real-world scenarios.

B. Results

The weather conditions during the experiments are summarised in Tab. I, based on meteorological data. This may differ slightly from local conditions; these could not be recorded due to the absence of required sensors. In-harbour tests were conducted under minimal disturbance as intended, while sea trials were conducted in relatively calm weather. More challenging conditions could have provided additional insight and more varied results.

The same metrics used in the simulation trials were applied to the field trials. However, no direct quantitative comparison was made between the simulation and the real world results under similar conditions due to differences in the reference trajectories, as explained in Appendix C.

As in the simulation study, both the PID and ADRC controllers were evaluated on trajectories performed in the harbour and at sea. For each controller and location, two trajectories were recorded, resulting in a total of eight trajectories. The results, summarised in Fig. 16 and Fig. 17, present the Cross-Track Error (XTE) and the total battery usage, respectively. Both metrics were averaged over the two recorded trajectories.

TABLE I
EXPERIMENTAL CONDITIONS OF FIELD TRIALS.

Experiment	Condition	Magnitude	Direction
In Harbour	Sea State	0-1	N/A
	Wind Speed	6 kts	SSW
	Current Speed	N/A	N/A
At Sea	Sea State	1-2	N/A
	Wind Speed	8 kts	SSE
	Current Speed	0.7 kts	SSW

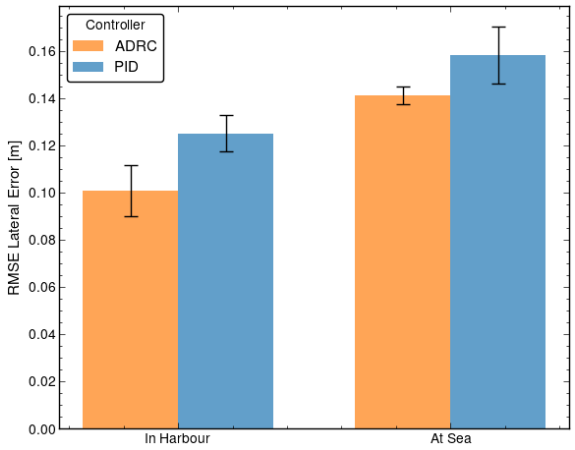

Fig. 16. RMS of the cross-track error (XTE) for each controller, averaged over two real-world trajectories. Error bars indicate the minimum and maximum measured values.

A sample of the recorded trajectories is shown in Fig. 18. These trajectories illustrate the controllers' performance during the two tests, with a zoomed-in view of the fifth corner of the trajectory, similar to the simulation results shown in Fig. 11.

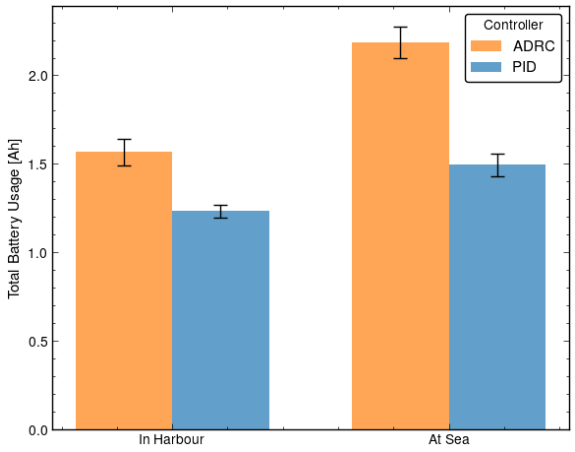

Fig. 17. Total battery consumption of each controller, averaged over two real-world trajectories. Error bars indicate the minimum and maximum measured values.

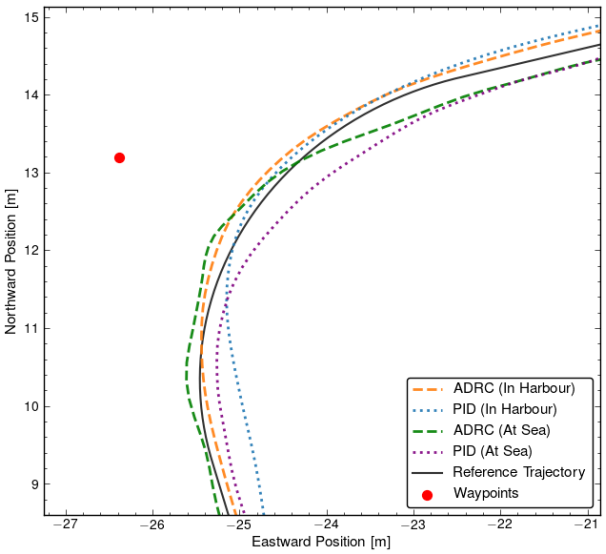

Fig. 18. Comparison of ADRC and PID controllers during field trials in the harbour and at sea.

C. Discussion

The results of the real-world tests reveal trends similar to those observed in simulation. As shown in Fig. 16 and Fig. 17, the ADRC controller achieves a reduction in XTE under all testing conditions, although this comes at the expense of increased battery consumption. However, the observed reduction in XTE is notably less pronounced than in simulation. This can be partly attributed to the increased turning radius of the reference trajectory, as discussed in Appendix C. The larger turning radius enables the slower PID controller to more effectively follow the reference trajectory, contributing to the lower XTE for both controllers compared to the simulation results.

The performance gap between the two controllers narrows further in sea trials. While the ADRC controller still outperforms the PID controller slightly, the worst-case XTE for ADRC is comparable to the best-case XTE for PID. Qualitative analysis of the trajectories in Fig. 18 reveals that the ADRC controller exhibits significant course corrections during corners at sea, repeatedly overshooting its heading and producing a zigzag pattern. This behaviour is absent in the PID controller, even though both experienced disturbances of similar magnitudes. These observations suggest that the ADRC controller may be overly aggressive, causing it to overshoot its own setpoint. This appears to be amplified by the presence of disturbances, as this behaviour is less observable during harbour trials.

These qualitative findings are corroborated by Fig. 17, which highlights a substantial increase in battery usage for the ADRC controller when transitioning from harbour to sea trials. Although an increase is also observed for the PID controller, it is far less pronounced. This indicates that the ADRC controller expends more energy to track the trajectory under the presence of similar disturbances.

VII. Conclusion

This study evaluated the performance of the ADRC framework for USV trajectory tracking through simulations and field trials. The results indicate that ADRC outperforms PID in reducing cross-track error in both simulation (by 30-40%) and field trials (by 10-20%). In field trials, this improvement was less pronounced due to the increased turning radius in the reference trajectory as shown in Appendix C, which resulted in lower cross-track errors for all controllers. This difference in the reference trajectory makes it difficult to directly attribute the performance differences to the controller itself. Future work should address this limitation by using identical reference trajectories, enabling direct quantitative comparisons between simulation and reality.

In addition to the reduction in cross-track error, ADRC exhibited increased energy consumption compared to PID. In simulation, this increase was observed only in the absence of current. With current present, ADRC completed the trajectory faster, resulting in equal battery usage. In field trials, the transition from harbour to near-shore conditions exacerbated this effect, with ADRC consuming approximately 50% more energy than PID. These findings suggest that while ADRC improves trajectory tracking, its higher energy demand may limit its suitability for industrial applications, where endurance is critical.

In conclusion, while ADRC offers improved performance, the trade-off with significantly increased energy consumption may be too great for practical use in industrial USV applications. Future research should aim to optimise the ADRC control framework to achieve a balance between performance and energy efficiency, focusing on tuning of controller parameters and performance at sea rather than in environments with few disturbances such as harbours or lakes.

Appendix A
Unity Simulation Verification

The Unity physics simulation was validated against the known manoeuvring dynamic model of the DUS V2500, shown in Fig. 19. Both the simulation and the dynamical model were subjected to identical raw motor inputs without an active controller, and their resulting trajectories were recorded over the same time duration. The first trajectory corresponds to a zigzag manoeuvre in the NED reference frame, where both stern thrusters were intermittently activated in the positive direction. The second trajectory represents a rotational manoeuvre, where opposing stern thruster inputs induce rotational motion without forward movement. This trajectory is presented in the time domain for clarity.

Appendix B
Trajectory Tracking with Modified Guidance Law

As shown in Fig. 11, the presence of current causes a consistent lateral offset in the trajectory due to limitations of the default L_1 guidance law. In this approach, the look-ahead point is fixed on the trajectory, and the USV attempts to reach it using the bow thruster. However, when the bow thruster's maximum output is insufficient to counteract the lateral forces

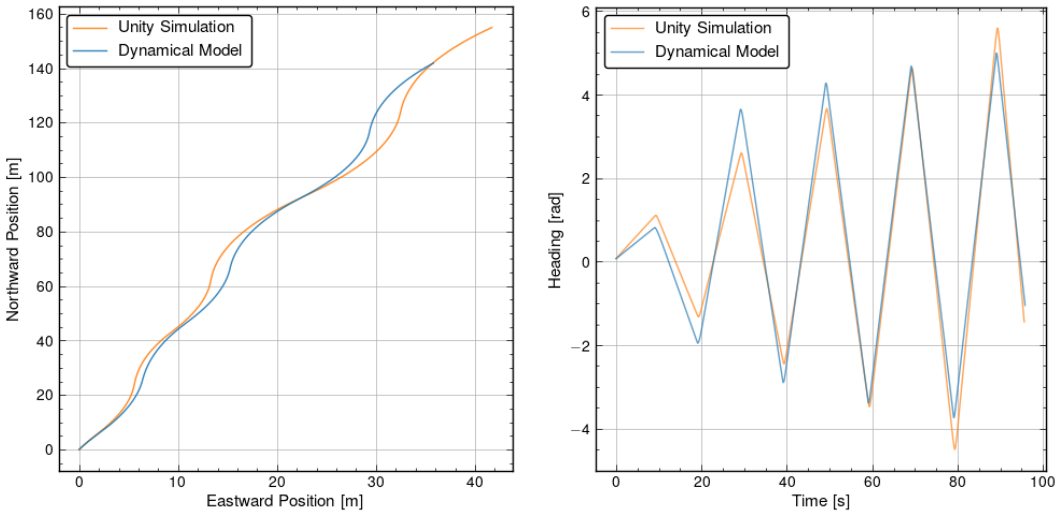

(a) Zigzag manoeuvre.

(b) Rotational spin manoeuvre.

Fig. 19. Verification of the Unity DWP2 physics simulation, compared to a known manoeuvring model.

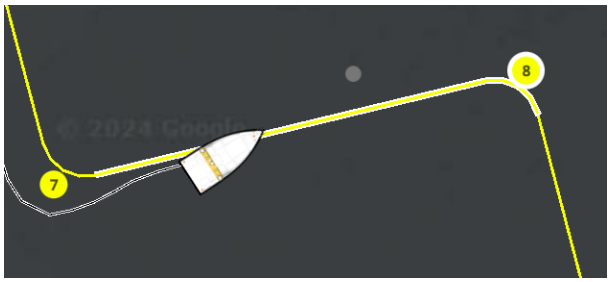

Fig. 20. Example of a PID controller used to shift the lookahead point in response to lateral offsets caused by external disturbances.

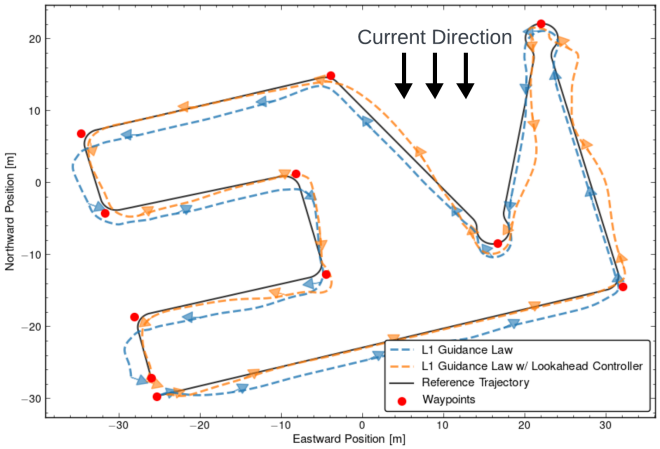

Fig. 21. Comparison of trajectory tracking performance between the default L_1 guidance law and a guidance law with a lookahead point controller. Both trajectories are exposed to a 0.5m/s current, with identical ADRC controllers applied. Arrows indicate USV heading.

from the current, the USV stabilises at an equilibrium offset away from the trajectory.

To address this issue, the look-ahead point can be shifted laterally, causing the equilibrium position of the USV to align with the desired trajectory. One method implemented on the DUS V2500 is to introduce a controller that adjusts the look-ahead point based on the lateral position of the vessel. As depicted in Fig. 20, a PID controller shifts the look-ahead point laterally, compensating for the current and closing the lateral offset.

The impact of this modified guidance law is shown in Fig. 21. It is apparent that with the modified guidance law the USV heading is not always aligned with the trajectory, indicating that the stern thrusters are used in conjunction with the bow thruster to compensate for the lateral offset. Although the adjusted guidance law eliminates the offset caused by current during straight-line tracking, it may lead to overcorrection and reduced performance in sharp corners. This suggests that gain-scheduling or an alternative tuning approach may be necessary to temporarily disable or adjust the controller in cornering scenarios.

Appendix C
Comparison of Simulation and Field-Testing

Although the waypoints that define the trajectory are identical between the simulation and real-world tests, the generated reference trajectories differ due to variations in the minimum allowed turning radius between the simulated and actual vessels, as illustrated in Fig. 22. The figure shows the vessel following the trajectory using an identical ADRC controller with the same parameters. The difference in turning radius hinders a direct comparison of results, but this can be resolved by conducting a further simulation study with an adjusted turning radius. It may also alter the results in simulation, as the PID controller is likely to perform better with a larger turning radius, as can be seen from the field-testing results. The use of different turning radii is a limitation of this study,

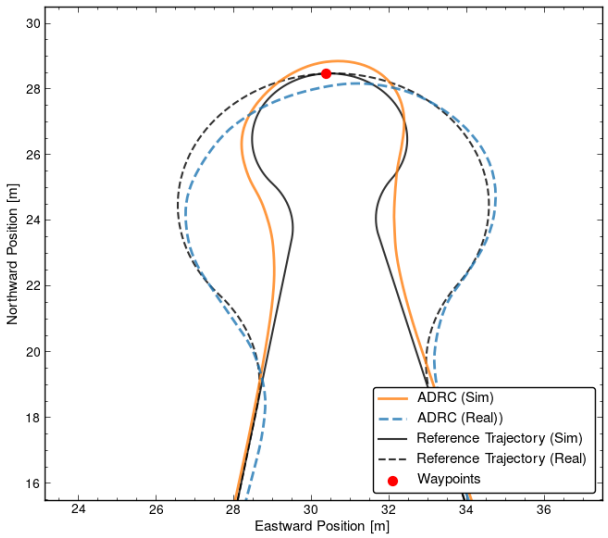

Fig. 22. Reference trajectories for simulation and real-world experiments. While the waypoints are identical, the minimum turning radius differs between the simulated and real vessel, affecting the generated trajectory.

and should be addressed in future works.

Acknowledgment

This study would not have been possible without the generosity of Demcon Unmanned Systems, who provided their time, access to existing systems and software, and made the V2500 available for testing in Scheveningen. A special thanks to the entire team for their invaluable support in preparing the vessel and assisting during the trials. We also express our gratitude to the TRiLOGy project for enabling collaboration between the Delft University of Technology and industry partners like Demcon Unmanned Systems, making this research possible.

References

[1] J. Yuh, G. Marani, and D. Blidberg, "Applications of marine robotic vehicles," *Intelligent Service Robotics*, vol. 4, pp. 221–231, 10 2011.

[2] J. H. Stel, *Exploring and Exploiting Deep Ocean Space*. Cham: Springer International Publishing, 2021, pp. 65–92.

[3] Z. Liu, Y. Zhang, X. Yu, and C. Yuan, "Unmanned surface vehicles: An overview of developments and challenges," *Annual Reviews in Control*, vol. 41, pp. 71–93, 2016.

[4] V. Bolbot, A. Sandru, T. Saarniniemi, O. Puolakka, P. Kujala, and O. A. Valdez Banda, "Small unmanned surface vessels—a review and critical analysis of relations to safety and safety assurance of larger autonomous ships," *Journal of Marine Science and Engineering*, vol. 11, no. 12, 2023.

[5] G. Roberts and R. Sutton, *Advances in Unmanned Marine Vehicles*. Advances in Unmanned Marine Vehicles, 01 2006.

[6] *How USVs can Change the Offshore Inspection Market Through Novel Operating Models*, ser. OTC Offshore Technology Conference, vol. Day 1 Mon, May 06, 2024, 05 2024.

[7] H. Xu and C. Guedes Soares, "Review of path-following control systems for maritime autonomous surface ships," *Journal of Marine Science and Application*, vol. 22, pp. 153–171, 07 2023.

[8] L. C. McNinch, H. Ashrafiuon, and K. R. Muske, "Optimal specification of sliding mode control parameters for unmanned surface vessel systems," in *2009 American Control Conference*, 2009, pp. 2350–2355.

[9] E. Børhaug, A. Pavlov, E. Panteley, and K. Y. Pettersen, "Straight line path following for formations of underactuated marine surface vessels," *IEEE Transactions on Control Systems Technology*, vol. 19, no. 3, pp. 493–506, 2011.

[10] T. I. Fossen, M. Breivik, and R. Skjetne, "Line-of-sight path following of underactuated marine craft," *IFAC Proceedings Volumes*, vol. 36, no. 21, pp. 211–216, 2003, 6th IFAC Conference on Manoeuvring and Control of Marine Craft (MCMC 2003), Girona, Spain, 17-19 September, 1997.

[11] B. Qiu, G. Wang, Y. Fan, D. Mu, and X. Sun, "Adaptive course control-based trajectory linearization control for uncertain unmanned surface vehicle under rudder saturation," *IEEE Access*, vol. 7, pp. 108 768–108 780, 2019.

[12] W. Liu, H. Ye, and X. Yang, "Model-free adaptive sliding mode control method for unmanned surface vehicle course control," *Journal of Marine Science and Engineering*, vol. 11, no. 10, 2023.

[13] J. Han, "From PID to active disturbance rejection control," *IEEE Transactions on Industrial Electronics*, vol. 56, no. 3, pp. 900–906, 2009.

[14] J. Hu, Y. Ge, X. Zhou, S. Liu, and J. Wu, "Research on the course control of USV based on improved ADRC," *Systems Science & Control Engineering*, vol. 9, no. 1, pp. 44–51, 2021.

[15] F. Chen, H. Xiong, and J. Fu, "The control and simulation for the ADRC of USV," in *2015 Chinese Automation Congress (CAC)*, 2015, pp. 416–421.

[16] Y. Fan, L. Liu, and Y. Yang, "ADRC course control for USV based on fuzzy self-tuning," in *2021 4th International Conference on Intelligent Autonomous Systems (ICoIAS)*, 2021, pp. 307–311.

[17] Y. Zheng, J. Tao, Q. Sun, H. Sun, Z. Chen, M. Sun, and G. Xie, "Soft actor–critic based active disturbance rejection path following control for unmanned surface vessel under wind and wave disturbances," *Ocean Engineering*, vol. 247, p. 110631, 2022.

[18] M. Fu, Q. Wang, Y. Wang, and Y. Xu, "Design of ADRC for unmanned surface vehicle heading based on immune particle swarm optimization," in *2021 IEEE International Conference on Mechatronics and Automation (ICMA)*, 2021, pp. 130–135.

[19] H. Li, H. Chen, N. Gao, N. Aït-Ahmed, J.-F. Charpentier, and M. Benbouzid, "Ship dynamic positioning control based on active disturbance rejection control," *Journal of Marine Science and Engineering*, vol. 10, no. 7, 2022.

[20] D. Wu, K. Yuan, Y. Huang, Z.-M. Yuan, and L. Hua, "Design and test of an improved active disturbance rejection control system for water sampling unmanned surface vehicle," *Ocean Engineering*, vol. 245, p. 110367, 2022.

[21] R. Skjetne, Øyvind Smogeli, and T. I. Fossen, "Modeling, identification, and adaptive maneuvering of CyberShip II: A complete design with experiments," *IFAC Proceedings Volumes*, vol. 37, no. 10, pp. 203–208, 2004, iFAC Conference on Computer Applications in Marine Systems - CAMS 2004, Ancona, Italy, 7-9 July 2004.

[22] C. Li, J. Jiang, F. Duan, W. Liu, X. Wang, L. Bu, Z. Sun, and G. Yang, "Modeling and experimental testing of an unmanned surface vehicle with rudderless double thrusters," *Sensors*, vol. 19, no. 9, 2019.

[23] X.-G. Wang, Z. Zou, F. Xu, and R.-Y. Ren, "Sensitivity analysis and parametric identification for ship manoeuvring in 4 degrees of freedom," *Journal of Marine Science and Technology*, vol. 19, 12 2014.

[24] A.-A. Al-Habashneh, C. Moloney, and E. Gill, "Ocean wave spectrum estimation from marine radar data using the polar Fourier transform," in *OCEANS 2014 - TAIPEI*, 2014, pp. 1–6.

[25] J. Zou, "Robust active disturbance rejection control scheme for quadrotor UAVs: Experimental prototyping," Master's Thesis, Eindhoven University of Technology, 8 2018.

[26] N. S. Nise, *Control systems engineering*. John Wiley & Sons, 2020, pp. 163, 667.

[27] B.-Z. Guo and Z. Zhao, *Active Disturbance Rejection Control for Nonlinear Systems: An Introduction*. John Wiley & Sons, 2016, pp. 93, 152.

[28] W. Abdul-Adheem, A. Azar, I. Ibraheem, and A. Humaidi, "Novel active disturbance rejection control based on nested linear extended state observers," *Applied Sciences*, vol. 10, p. 4069, 06 2020.

[29] Q. Zheng, Z. Chen, and Z. Gao, "A practical approach to disturbance decoupling control," *Control Engineering Practice*, vol. 17, no. 9, pp. 1016–1025, 2009.

[30] J. Wang, H. Zhang, G. Xiao, Z. Dan, S. Zhang, and Y. Xie, "A comparison study of tracking differentiator and robust exact differentiator," in *2020 Chinese Automation Congress (CAC)*, 2020, pp. 1359–1364.

3

Simulation Design

As outlined in Chapter 2, a Unity-based simulation was employed to validate the controller's performance prior to conducting field trials. This simulation interfaces with a digital twin of the onboard control computer. Key components of the simulation, including the Scheveningen environment, sensor simulation (GPS and IMU), and the communication protocol with the control computer, were developed in-house by Demcon. Building on this framework, this thesis introduces several new features, which are summarised in this chapter.

First, Section 3.1 provides an overview of the dynamic physics simulation that forms the foundation of the simulation environment. The modelling of disturbances and their interaction with the physics simulation is also detailed in Section 3.1. Lastly, Section 3.3 presents an overview of developments made for user interaction, such as creating disturbances, interacting with the vessel, and other quality-of-life improvements.

3.1. Physics Simulation

A key contribution of this thesis is the integration of a dynamic physics simulation using the Dynamic Water Physics 2 (DWP2) package into the Unity simulation of DUS. This package simulates buoyancy and hydrodynamic forces based on mesh data as shown in Figure 3.1, replacing the prior manoeuvring model derived from system identification data. The switch to a physics-based approach was motivated by the following advantages:

- **Ease of vessel integration**: A physics simulation using DWP2 is based solely on mesh data, enabling the straightforward inclusion of new vessels as long as a 3D model is available.
- **6-DOF simulation**: Traditional manoeuvring models are limited to three Degrees-of-Freedom (DOF) (surge, sway, and yaw). Modelling additional DOF (roll, pitch, and heave) requires experimental setups such as wave tanks to identify model dynamics for remaining DOF. The physics simulation provides an effective alternative for estimating these effects.
- **Interaction with water renderers**: The DWP2 package integrates well with various Unity ocean and water rendering systems, allowing for vessel-wave interactions to be easily implemented.

As the forces acting on the vessel are calculated based on the mesh, a high-quality model is required to ensure accurate force calculations. A 3D mesh was obtained from a CAD model of the DUS V2500, then converted and imported into the Unity simulation. This mesh is shown on the left in Figure 3.2. However, the original mesh contains an excessive number of vertices and small surfaces that do not significantly contribute to hydrodynamic forces. This complexity can lead to reduced simulation performance and less reliable physics calculations.

To address this issue, a simplified mesh was manually constructed, consisting of only the primary components of the hull. DWP2 further combines similar faces of this mesh to improve computational efficiency. This simplified mesh maintains the necessary fidelity for accurate force modelling while reducing computational overhead.

In the Unity simulation, the user exclusively sees the standard 3D model of the vessel, but all

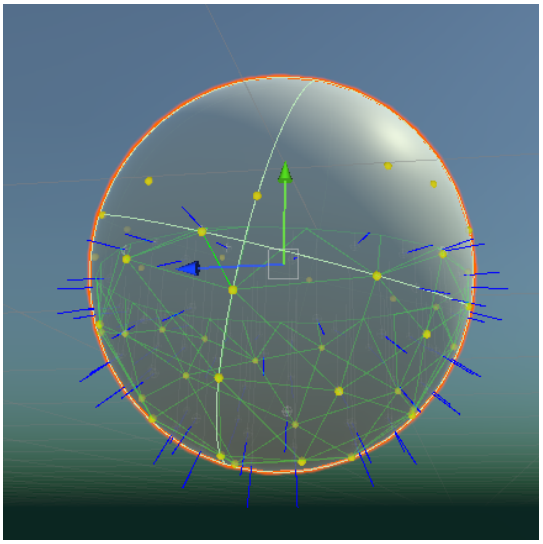

Figure 3.1: Mesh-based buoyancy calculations using DWP2, with each blue arrow representing a force acting on a mesh face.

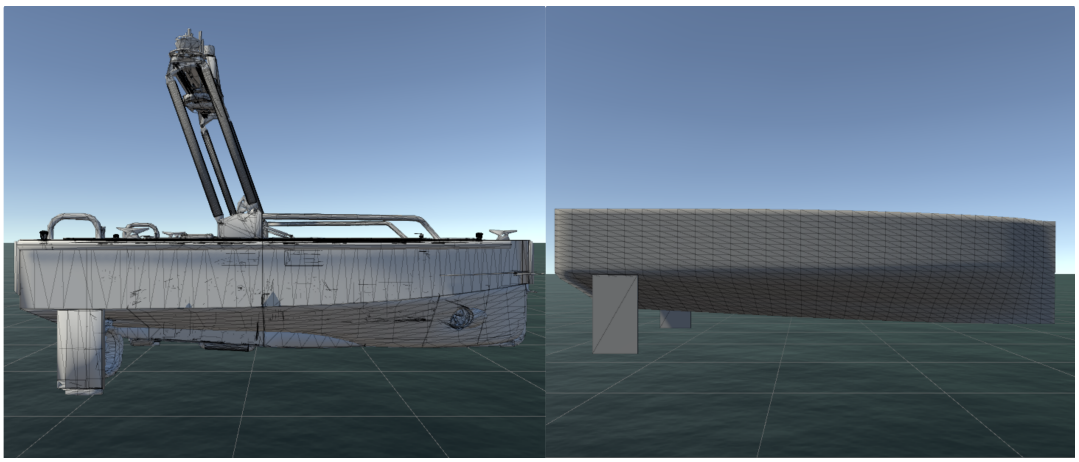

Figure 3.2: Comparison of the standard 3D mesh of the DUS V2500 (left) and the simplified mesh used by DWP2 (right).

hydrodynamic forces are calculated and applied to the simplified mesh. Unity's built-in `RigidBody` system applies the mass, moment of inertia, and centre of gravity of the vessel to the USV, in accordance with the known physical properties of DUS V2500.

The usage of DWP2 allows for the integration of most Unity-based ocean renderers. These wave renderers displace the water surface, and DWP2 calculates the hydrodynamic forces as the vessel interacts with these displacements. This setup allows for the simulation of vessel dynamics under various wave conditions without requiring predefined models obtained via system identification.

It is important to note that while DWP2 models hydrodynamic forces, it does not account for the momentum transfer from a wave to the vessel. Instead, it simulates the vessel's response based on the buoyancy and hydrodynamic forces experienced as the vessel interacts with the displaced ocean surface.

3.2. Disturbance Simulation

To complement the physics simulation discussed in Section 3.1, the open-source CREST 4 ocean renderer was selected to implement a realistic wave spectrum and fluid model to simulate currents. This package integrates with DWP2, enabling the creation of realistic maritime environments to which the vessel dynamically reacts.

CREST 4 serves two primary purposes. First, it facilitates the definition of a realistic wave spectrum

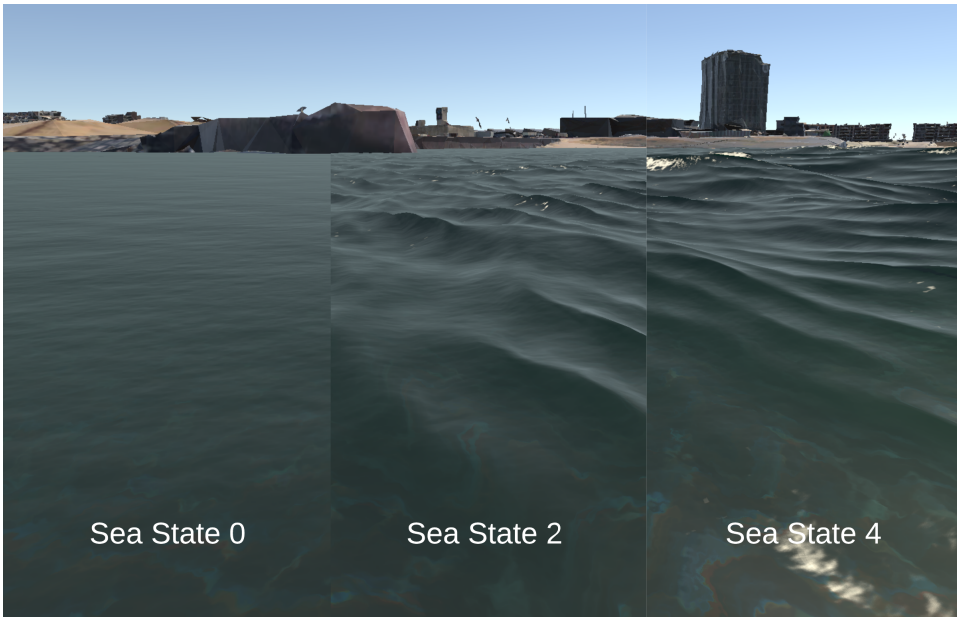

Figure 3.3: Comparison of different sea states, based on the Pierson-Moskowitz spectrum, created using the CREST 4 package.

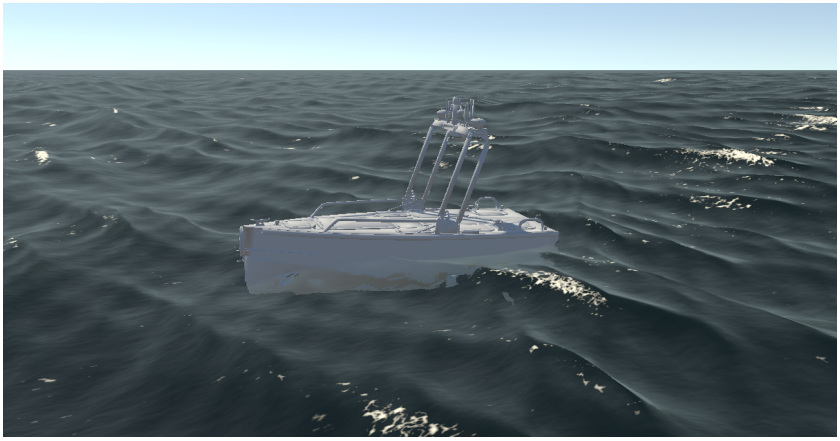

Figure 3.4: DUS V2500 operating in a simulated sea state 4.

that the vessel encounters, and second, it can be employed as a fluid simulation to model the effects of current on the vessel. In addition, wind disturbances were implemented separately to complete the disturbance simulation. The following sections provide an overview of these disturbance models.

3.2.1. Waves

While CREST 4 allows all components of the wave spectrum to be customised, this simulation employs the standard Pierson-Moskowitz spectrum, which represents a fully developed sea. The intensity of the wave spectrum can be adjusted to achieve the desired sea state, defined by the maximum wave height as seen in Section 3.3. For example, a sea state of 4 on the Douglas Sea Scale corresponds to a maximum wave height of 2.5 metres. A visual comparison of different sea states is shown in Figure 3.3, and the vessel operating in a simulated sea state 4 is shown in Figure 3.4.

As discussed in Section 3.1, these waves are modelled as vertical displacements of the water surface. Although buoyant and hydrodynamic forces are accurately calculated, the waves do not transfer momentum to the vessel, nor is their motion influenced by the vessel. This limitation can cause the vessel to appear partially submerged when encountering large waves. To address this, a clipping mesh is integrated above the vessel, removing any fluid volume above it when submerging occurs. This

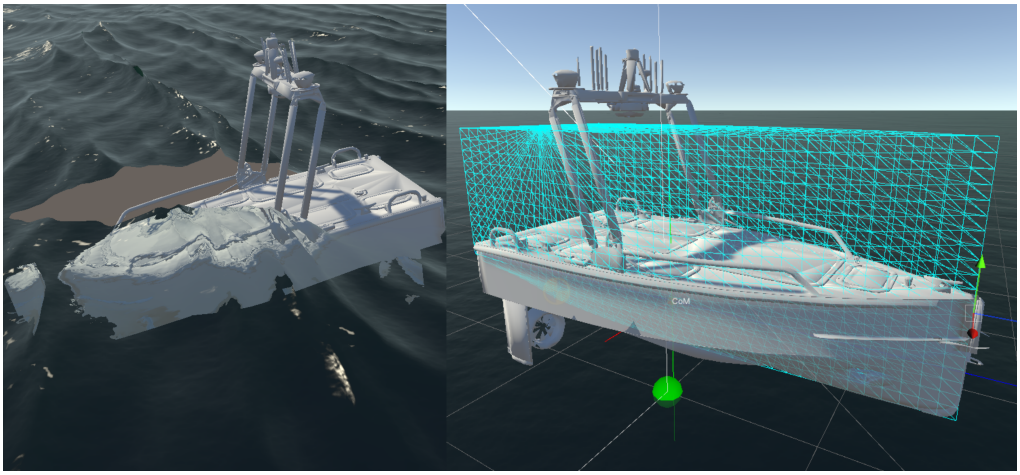

Figure 3.5: Example of a clipping mesh, removing water from above the vessel to avoid submersion when encountering waves head-on.

approach, illustrated in Figure 3.5, improves both the graphical fidelity, preventing the vessel from appearing to sink, and the simulation dynamics, as the vessel does not experience forces as if it were submerged.

3.2.2. Current

The CREST 4 package is also used to simulate fluid flow, enabling the implementation of realistic water currents. Fluid flow is applied to the water surface using a UV shader, where each channel encodes the fluid velocity in one direction, resulting in a 2D velocity field.

This UV shader is applied only to the water surface surrounding the USV, as currents outside this immediate area do not significantly affect the simulation. The shader is dynamically centred on the USV's position and updates as the vessel moves. This avoids the computational overhead of applying fluid flow to the entire water surface. An example of this implementation is shown in Figure 3.6, where the dimensions of the shader are significantly reduced for visualisation purposes.

While the CREST 4 current model supports the definition of non-uniform flow patterns, the implementation for this thesis is limited to currents with a uniform direction and velocity. This maintains simplicity for users when defining environmental disturbances, as described in Section 3.3. In addition, uniform currents represent most real-world scenarios in which the flow appears to have a uniform direction in the immediate operational area of the vessel.

3.2.3. Wind

Wind effects are modelled using the `HullWindApplicator` feature of the DWP2 package. This feature enables the creation of a simplified rectangular bounding shape around the non-submerged portion of the USV. The projected area A_p of the vessel with respect to the wind direction, as depicted in Figure 3.7, is used to calculate the total wind drag force F_D:

$$F_D = \frac{1}{2} C_D A_p V_w^2 \tag{3.1}$$

Here, C_D is the drag coefficient of the USV, and V_w is the freestream wind velocity. The drag coefficient C_D is approximated as 0.93, representing the average value of a cube angled with respect to the flow and a cube orientated perpendicular to the flow [21]. The freestream wind velocity is set by the user via the interface shown in Section 3.3.

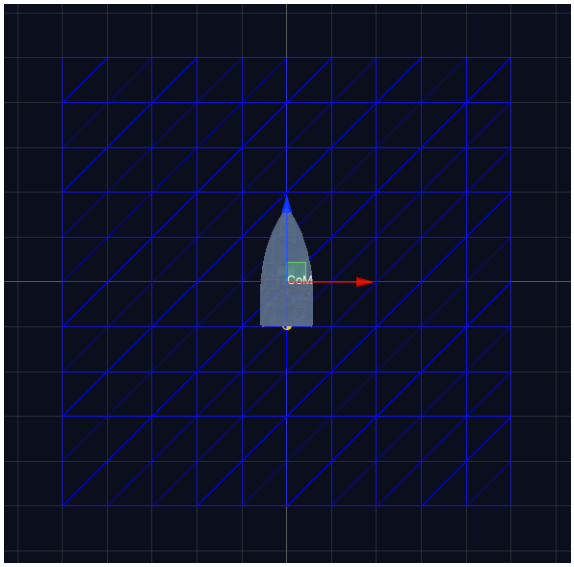

Figure 3.6: UV shader applying a fluid velocity around the vessel. The shader is automatically centred on the USV's position. Dimensions of the shader are reduced for visualisation purposes.

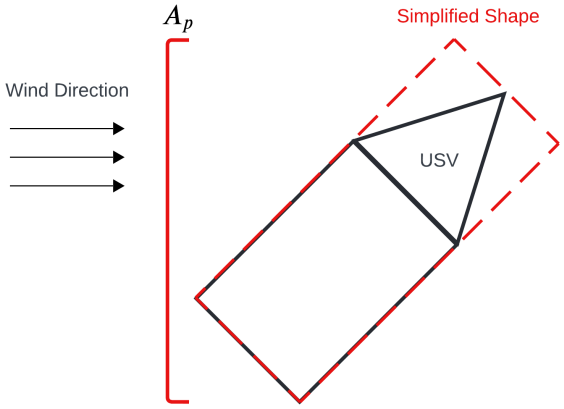

Figure 3.7: Projected area of the USV used to calculate wind force and direction, relative to the incoming wind.

3.3. Configuration and User Interaction

Several features aimed at improving and enabling user interaction for the Unity simulation were developed throughout this thesis. Firstly, a menu was added to enable and configure the simulation of physics presented in Section 3.1, allowing the user to control some key parameters. A menu was also added to define and configure the disturbance simulation as presented in Section 3.2. Furthermore, the old camera system was overhauled to improve the general usability of the simulation.

3.3.1. Simulation and Physics Settings

The physics simulation described in Section 3.1 replaces the preexisting manoeuvring model used to simulate the dynamics of the vessel. While this allows the vessel to interact with the disturbance simulation, there may be scenarios where reverting to the old manoeuvring model is desired. Consequently, an option was added to dynamically toggle between the two models, enabling verification of the DWP2 physics simulation as outlined in Chapter 2. This toggle is shown in Figure 3.8.

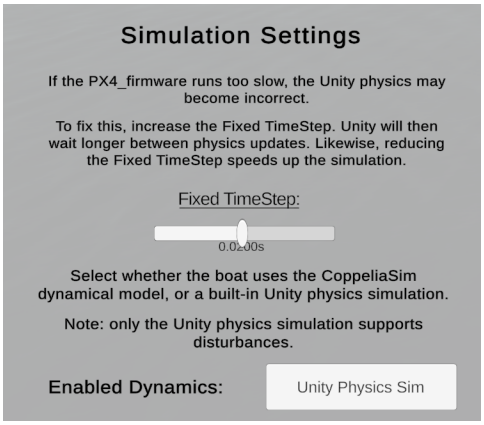

Figure 3.8: Simulation settings menu of the Unity simulation, allowing users to toggle between the manoeuvring model and the physics simulation described in Section 3.1.

Additionally, a slider is provided to define the `Fixed TimeStep`, the frame-rate-independent interval

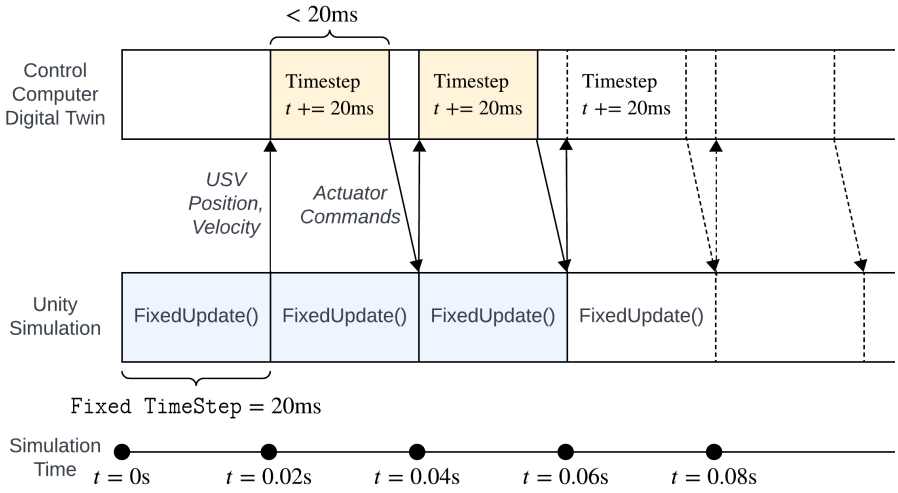

Figure 3.9: Communication between the control computer digital twin and Unity simulation.

that dictates how often physics calculations and the `FixedUpdate()` function are triggered. This function handles critical operations such as applying thrust to the USV using actuator commands from the control computer's digital twin or transmitting the USV's position back to the control computer. An overview of this communication process is provided in Figure 3.9.

As shown in Figure 3.9, `Fixed TimeStep` directly influences the simulation speed. The control computer is simulated with a fixed timestep of 20 ms, transmitting actuator commands to Unity. These commands must arrive before the end of `FixedUpdate()`, as delays would prevent the vessel's forces from being updated correctly. Given that control calculations are completed in under 20 ms, a `Fixed TimeStep` of 20 ms achieves a Real-Time Factor (RTF) of 1, where the simulation runs in sync with real life.

Likewise, `Fixed TimeStep` can be reduced - given the duration remains longer than the control computer update time - to achieve an RTF greater than 1, enabling the simulation to run faster than real time. Conversely, on slower systems where control computations require more time, `Fixed TimeStep` can be increased to slow down the simulation and ensure `FixedUpdate()` is triggered only after actuator commands are received, preventing errors in force application.

3.3.2. Disturbance Controls

The disturbance simulation described in Section 3.2 must be configurable by the user during the simulation. The configuration menu is shown in Figure 3.10 and provides options for adjusting wave, wind, and current disturbances within the simulation.

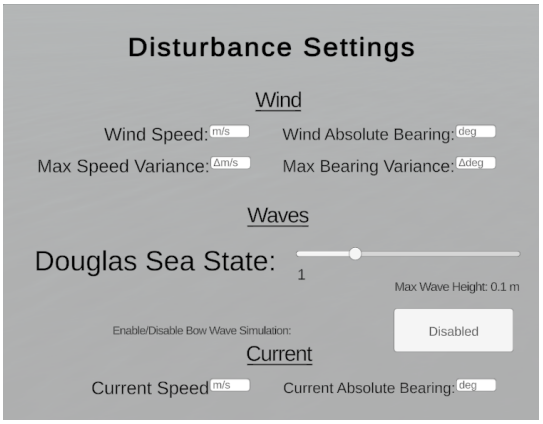

Figure 3.10: Disturbance configuration menu of the Unity simulation.

Code	Wave Height (m)	Characteristic Name
0	0.0	Calm (Glassy)
1	0.0 – 0.1	Calm (Rippled)
2	0.1 – 0.5	Smooth
3	0.5 – 1.25	Slight
4	1.25 – 2.5	Moderate
5	2.5 – 4.0	Rough
6	4.0 – 6.0	Very Rough
7	6.0 – 9.0	High
8	9.0 – 14.0	Very High
9	> 14.0	Phenomenal

Figure 3.11: Douglas Sea Scale and corresponding wave heights [22].

Although CREST 4 allows for alterations to individual frequency components of the wave spectrum, this level of control is unnecessary for most users. Instead, the spectrum is predefined as the Pierson-Moskowitz spectrum, with user control limited to adjusting the total spectrum intensity. The intensity is subdivided by sea states based on the Douglas sea scale, as illustrated in Figure 3.11. The corresponding wave heights are also included in the disturbance menu, enabling users to quickly assess and set the wave intensity for their simulation. This combination of a predefined spectrum and an adjustable intensity ensures a user-friendly configuration of the desired disturbances.

Wind settings are similarly configurable within the disturbance menu. Users can specify the absolute bearing and wind speed using input fields. Since wind speed and direction are generally non-uniform, users can define maximum variance for both characteristics. Wind characteristics will then vary randomly within the specified range during the simulation. Furthermore, the wind direction influences the wave direction, reflecting their natural coupling in real environments. The settings for current disturbances are more straightforward, with users specifying speed and bearing. These settings apply a uniform flow to the water around the USV, as depicted in Figure 3.6.

3.3.3. Camera Controls

Although not essential for the collection of results in this thesis, the preexisting camera system exhibited limited functionality. To help create figures such as Figure 3.3 and Figure 3.4, a new camera system was developed to improve user control.

The updated system includes mouse and keyboard controls to directly pan, zoom, and move the camera around the vessel or freely throughout the simulation. By default, the camera follows the USV, and a re-centre button was added to allow users to quickly reset the camera position to the USV. The improved camera controls and settings are shown in Figure 3.12.

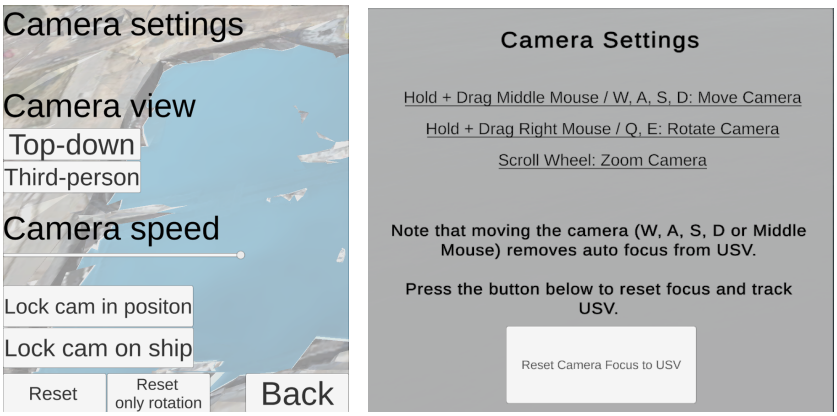

(a) Camera settings before overhaul. **(b)** Camera settings and controls after overhaul.

Figure 3.12: Comparison of camera settings and controls before and after the overhaul to enhance user interaction within the simulation.

4

Additional Simulation Results and Discussion

This chapter presents additional simulation results that build upon the analysis provided in Chapter 2, while offering a further discussion on the performance of the ADRC framework under various operating conditions. Several aspects of the controller that were not explored in Chapter 2, such as velocity tracking, as well as a more detailed analysis of results that could not be included previously, are addressed in this chapter.

First, Section 4.1 evaluates the controller velocity tracking performance in both calm waters and wave disturbances, including a comparison with the baseline PID controller. Strategies to improve tracking efficiency, such as a novel high-frequency damping approach, are also examined. Next, Section 4.2 analyses the increased control effort associated with ADRC, identifying contributing factors and proposing potential improvements. In Section 4.3, a detailed discussion of the L_1 guidance law and the lateral offset experienced under current disturbances is provided. Finally, Section 4.4 discusses the challenges of parameter tuning within the ADRC framework, and the applicability of self-tuning algorithms for industrial control applications.

4.1. Velocity Tracking

While Chapter 2 provides a detailed analysis of the vessel's tracking performance, measured via the Cross-Track Error (XTE), limited insight is given into velocity tracking performance. As shown in Figure 4.1, the trajectory information includes velocity set points that define the mission speed, typically set to 1.4m/s by default, with reductions near the corners to reduce the turning radius. The following section elaborates on the velocity tracking controller's performance, first in calm conditions, and then in environments with wave disturbances.

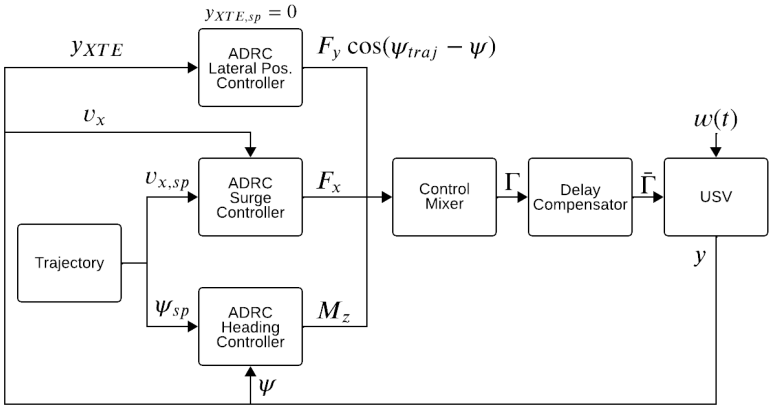

Figure 4.1: Trajectory tracking controller design using the ADRC framework. Trajectory information contains velocity setpoints, including the mission speed and reductions for cornering.

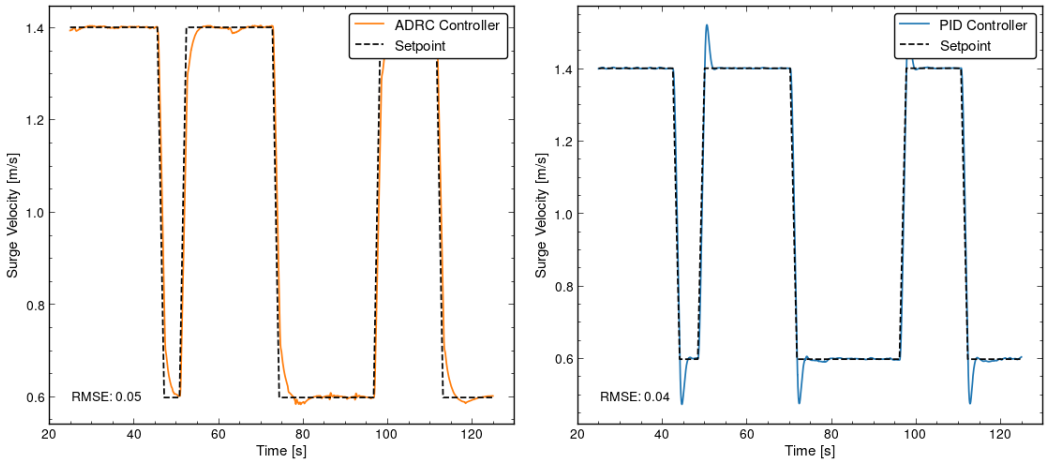

Figure 4.2: Velocity tracking performance of both controllers. No disturbances act on the vessel.

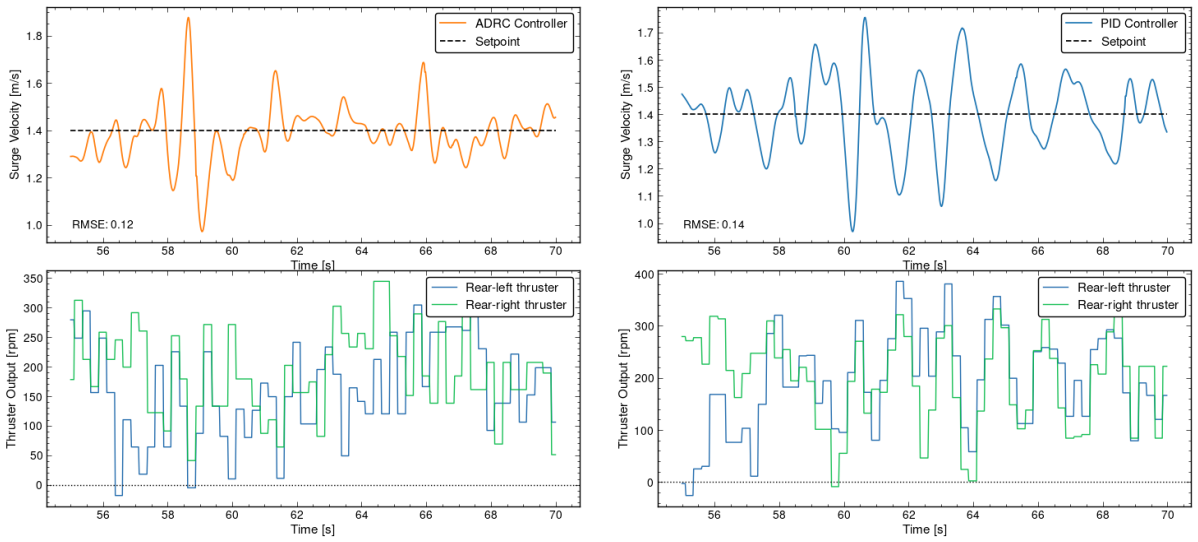

Figure 4.3: Velocity tracking performance of both controllers in a simulated Sea State 4. Plots are focused on a section of the trajectory with a constant mission speed.

4.1.1. Velocity Tracking in Calm Conditions

In the absence of disturbances, the velocity tracking performance of the simulated vessel is compared between the ADRC and baseline PID controllers. The resulting surge velocity is compared to the setpoint using the Root Mean Square Error (RMSE) between the signals to evaluate their performance. These results are summarised in Figure 4.2.

From these results, it is evident that while the PID controller achieves a smaller RMSE, this is primarily due to aggressive tuning, resulting in overshoot. The ADRC controller, while settling more slowly, avoids overshooting the setpoint, thus minimising control effort. Despite these differences, both controllers show sufficient performance, with quick convergence to the required speed in disturbance-free conditions.

4.1.2. Velocity Tracking in Sea State 4

In environments with disturbances, the velocity tracking performance is significantly impacted. The simulated vessel is exposed to Sea State 4, and the velocity tracking results are summarised in Figure 4.3. A segment of the trajectory is shown where a constant mission speed of 1.4m/s is maintained.

In this scenario, significant fluctuations can be observed around the mission speed. The disturbance rejection capabilities of ADRC are clearly visible, as it outperforms the PID controller in maintaining the

desired velocity despite the waves. However, when the Rotations Per Minute (RPM) values of the stern thrusters are considered, it is apparent that both controllers have significant fluctuations in their control effort. In some instances, the thrusters even cross zero and provide backward thrust.

Such fluctuations occur when the vessel encounters a wave, which increases drag and causes the vessel to slow down. In response, the motors increase their output. Once the wave passes, the drag decreases and the vessel speeds up. The motors, attempting to maintain the set speed, reduce their output, sometimes even reversing, causing the observed fluctuations. This is a significant waste of energy, as the vessel will slow down automatically when encountering the next wave.

4.1.3. Gain Scheduling for Improved Velocity Tracking Efficiency

In situations similar to those described in the previous section, the disturbance rejection capabilities of ADRC work actively against it, as accurate tracking of the setpoint results in wasted energy. Instead, a desirable controller maintains constant thrust, which would result in maintaining the mission speed in the absence of disturbances. As waves are periodic, the vessel may slow or accelerate, but the mean velocity would remain at the setpoint.

In order to achieve improved velocity tracking efficiency, there are two approaches. Firstly, Demcon Unmanned Systems (DUS) developed a feature that avoids zero-crossing of the control output during sailing at a constant mission speed, which avoids situations where the thrusters act in the opposite direction of the direction of travel. This helps avoid the extreme case of energy wastage, but does not resolve the vessel constantly adjusting its control output to maintain the setpoint. This strategy could not be properly tested in simulation before adding wave disturbances, such as those shown in Section 3.2, and could only be evaluated in field trials. The development of this simulation allows for this implementation to be easily validated.

An alternative approach is to introduce an additional damping term to the control law. The ADRC control law will be used for the following experiment, although these techniques can apply to both controllers. The control law is modified as follows:

$$\begin{cases} e_1 = v_1 - z_1 \\ e_2 = v_2 - z_2 \\ u_0 = \text{fhan}(e_1, ce_2, r_1, h_1) \cdot \exp -\omega_d e_2^2 \\ u = -\frac{u_0 + z_3}{b_0} \end{cases} \tag{4.1}$$

Where ω_d controls how sharply the control output is damped when e_2 increases. This will logically reduce tracking performance, but aims to improve the efficiency of the controller as a trade-off. As it limits setpoint tracking performance, it should only be enabled when sailing with a constant velocity setpoint, similar to the zero-crossing avoidance feature developed by DUS.

The newly developed Unity simulation allows these two techniques to be compared directly. In Figure 4.4, the two methods mentioned above are compared to a standard ADRC implementation. All simulations show the vessel sailing in Sea State 4 in head seas. The battery capacity consumption is calculated over the length of the trajectory, while Figure 4.4 shows only a small segment of the trajectory.

From the results presented in Figure 4.4, the zero-crossing avoidance strategy is clearly seen to limit the force demands of the velocity controller to positive values. It must be noted that this does not limit the thrusts to strictly positive values, as torque demand can still result in negative thrust outputs. The introduction of this zero-crossing avoidance results in reduced tracking performance, as expected. However, this reduced performance is not nearly as severe as that observed with the high-frequency damping approach.

The high-frequency damping controller reacts much more slowly as the changes in e_2 are damped out. Although this results in a smoother control signal, the inability of the controller to use speed boosts from waves to reduce thruster requirements actually leads to increased energy consumption. Consequently, the zero-crossing avoidance method, as developed by DUS, is the most applicable solution in this case, as it saves energy compared to both the default ADRC implementation and the high-frequency damping implementation.

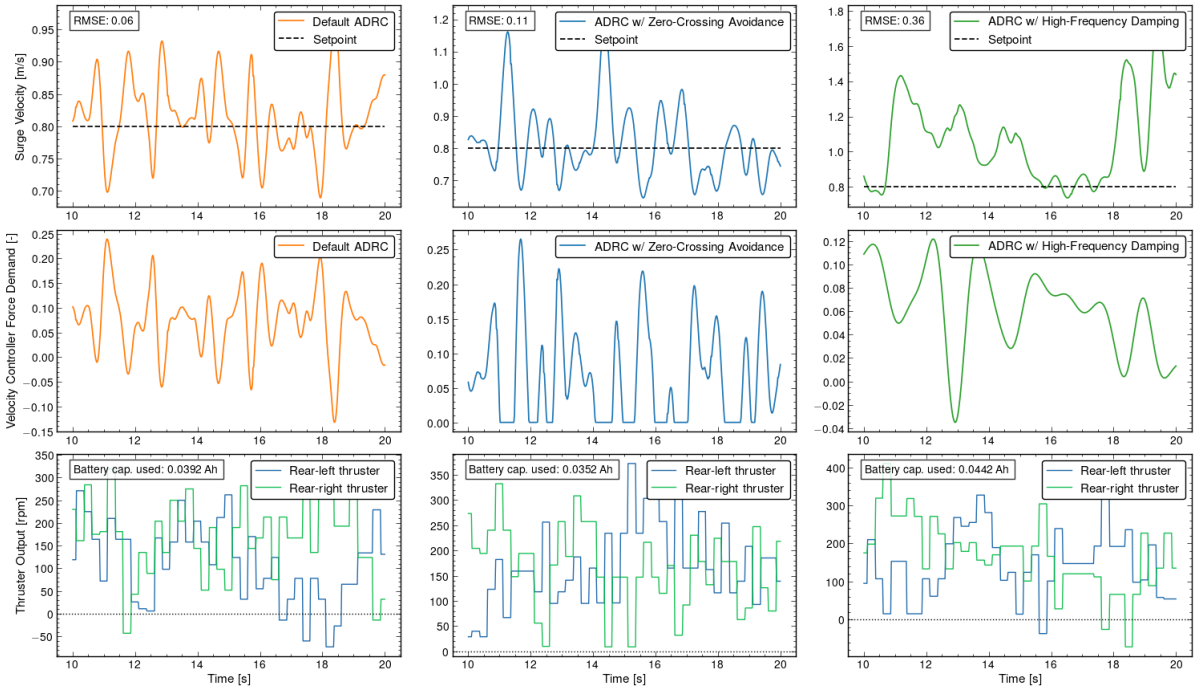

Figure 4.4: Comparison of (1) the default ADRC implementation, (2) zero-crossing avoidance of the surge force demand as developed by DUS, and (3) the proposed high-frequency damping approach, for a simulated USV sailing in sea state 4.

4.2. Increased ADRC Control Effort

In Chapter 2, it was observed that while ADRC reduced the XTE across all scenarios, it resulted in greater battery consumption in disturbance-free conditions. In scenarios with current, the battery consumption was similar for both controllers, but this can be attributed to ADRC's shorter trajectory due to its superior tracking performance. The increased control effort can be illustrated by the RPM values of a stern thruster during the start of a simulated trajectory without disturbances, as shown in Figure 4.5. In the following sections, the causes of this increased control effort are discussed first, followed by adjustments that can be made to resolve these issues.

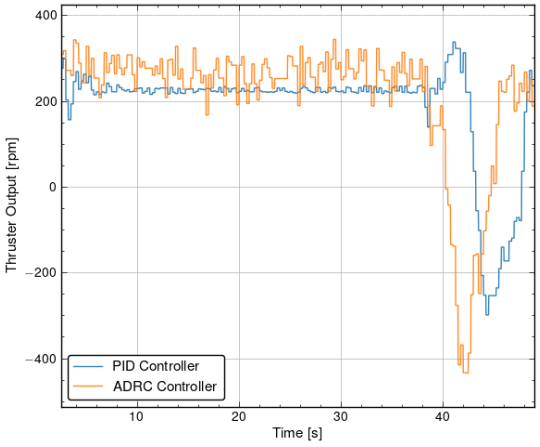

Figure 4.5: Comparison of RPM values for a stern thruster during a disturbance-free simulated trajectory. ADRC exhibits increased noise and a higher average RPM output compared to PID.

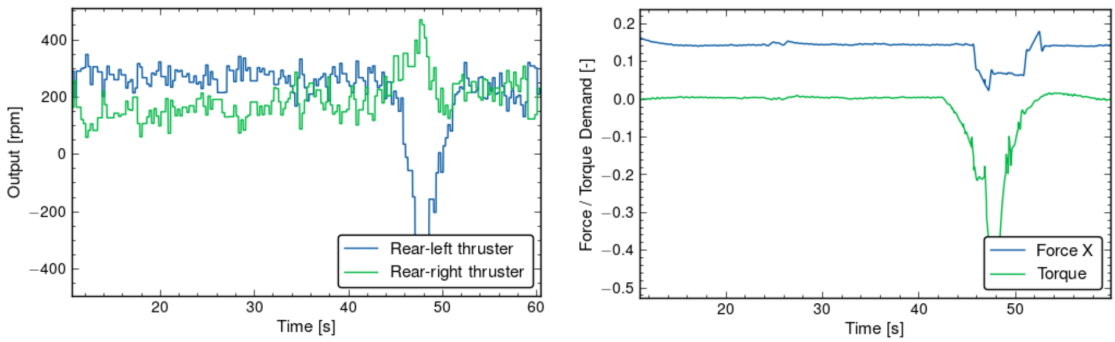

Figure 4.6: Comparison of the heading controller's torque output with stern thruster RPMs after applying the control mixer. Noise amplification highlights the effects of underactuation and ADRC's disturbance rejection strategy.

4.2.1. Contributing Factors

As seen in Figure 4.5, ADRC introduces more noise in the control signal compared to PID, and its average RPM output is higher. This increased output causes the vessel to reach sharp corners in the trajectory sooner, indicated by a significant decrease in motor output during a manoeuvre. However, this improvement comes with higher energy demands.

The underlying causes of this increased control effort are twofold. Firstly, the fundamental principle of ADRC involves compensating for the "total disturbance" $F(x_1, x_2, w(t), t)$. This disturbance encompasses both internal system dynamics and external influences, and since ADRC does not differentiate between these components, it actively compensates for internal system dynamics as if they were disturbances. This leads to a more aggressive control effort and higher energy consumption.

Secondly, noise in the control signal is significantly amplified by the vessel's control mixer. As shown in Figure 4.6, the stern thrusters, which are responsible for both surge and torque force production, exhibit significant noise in their RPM outputs, while the input force and torque requirements are significantly less noisy. As the vessel is underactuated, these thrusters respond to very small variations in the torque signal, which result in amplified changes in the stern thruster RPM signal.

4.2.2. Controller Tuning for Improved Efficiency

As described in Chapter 2, while alternative control mixer designs could address the noise amplification issue, additional solutions were also explored during this thesis. As the PID RPM signal in Figure 4.5 is relatively smooth with the same mixer, suggesting that further smoothing the ADRC torque and forward velocity signals could mitigate the issue without requiring alterations to the mixer.

To investigate whether the controller can be tuned to generate smoother outputs without compromising tracking performance, a sensitivity analysis was conducted on parameters of the heading controller's error-feedback function. This controller has the most significant impact on tracking performance and XTE. The parameters included in this analysis are:

- **Tracking speed** r_1: Determines the rate at which the controller converges to the setpoint.
- **Filter factor** h_1: Applies filtering to the control output, with larger values producing smoother and more filtered but slower responses.
- **Damping factor** c: Specifies the level of damping within the controller.

Each parameter was varied by ±50% relative to the default simulation values provided in Chapter 2. The effects of these variations were evaluated based on tracking performance, defined as the Root Mean Square (RMS) of the XTE, and the noise level in the stern thruster RPM signal. The noise in the RPM signal was quantified using the Mean Absolute Deviation (MAD), calculated as:

$$MAD_{\text{window}} = \frac{1}{N} \sum_{i=1}^{N} |x_{\text{rpm}}(i) - \mu_{\text{window}}| \tag{4.2}$$

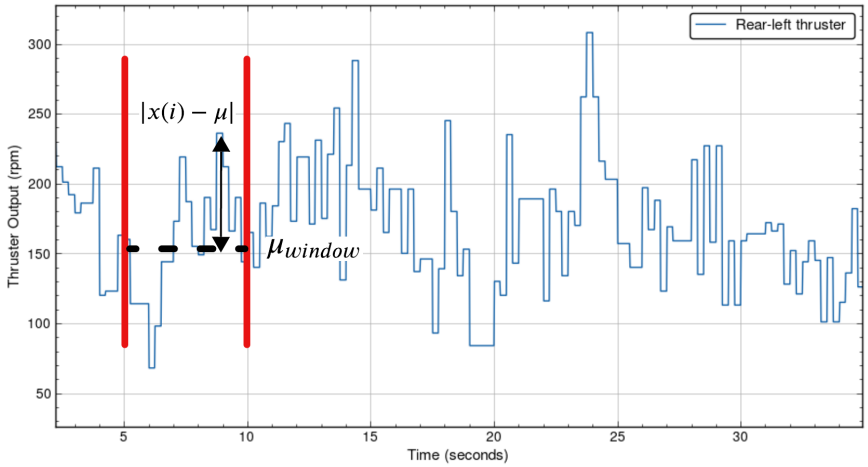

Figure 4.7: Calculation of Mean Absolute Deviation to assess the noisiness of the RPM output signal of a thruster using a sliding window.

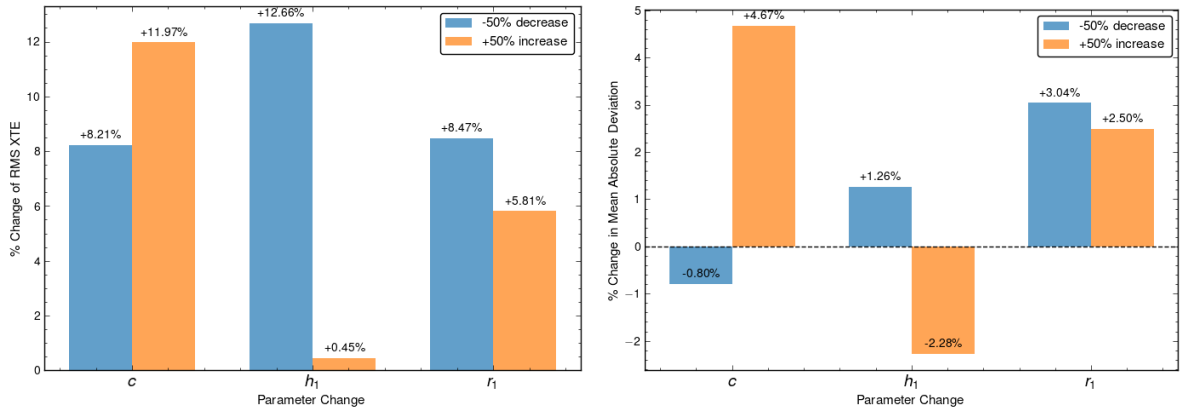

(a) Effect on tracking performance.

(b) Effect on RPM noise level measured via a sliding-window MAD.

Figure 4.8: Sensitivity analysis of the ADRC controller, comparing tracking performance with noise levels in the RPM output signal of a single stern thruster. All controllers were evaluated on the same trajectory under disturbance-free conditions, and compared to the default ADRC gains used in the simulation study.

This approach uses a sliding window to compute local MAD values, quantifying how much the signal varies over a small period of time, as shown in Figure 4.7. A smoother signal, characterised by fewer oscillations, is preferred, reflected by a lower MAD. The local MAD values were aggregated and averaged over the entire trajectory. The analysis was carried out for a single thruster, with the assumption that a reduction in noise would similarly affect both stern thrusters. The results of the sensitivity analysis, evaluating the effects of parameter variations on both the XTE and the noise in the stern thruster RPM, are presented in Figure 4.8.

From these results, it is evident that all parameter variations result in reduced tracking performance, except for an increase in the filter factor h_1, which has a minimal impact on the XTE. Although the variations of ±50% represent substantial parameter changes, these results suggest that the current parameter configuration is at least close to a local minimum in terms of tracking performance.

In terms of noise in the RPM output signal, increasing the filter factor h_1 is the only parameter adjustment associated with a reduction in noise. As this change is coupled with a negligible increase in XTE, it is clearly a favourable tuning decision. All other parameter variations resulted in an increase in XTE, accompanied by increased or negligible changes in the noise level of the RPM output signal.

4.3. Trajectory Offset from Current Disturbances

In Chapter 2, the offset observed during trajectory tracking of a USV under current disturbances was discussed. Although it is evident that the current pushes the vessel away from the trajectory in the direction opposite to the current, the reason for this offset being constant and identical for both controllers is less clear. In the appendix of Chapter 2, it was shown that introducing an additional controller to move the look-ahead point of the guidance law can help mitigate this offset; however, this approach also demonstrated drawbacks during cornering.

This section elaborates on the root cause of this phenomenon and its relationship to the default L_1 guidance law. The L_1 guidance law, commonly implemented for trajectory tracking in aerial vehicles, positions the look-ahead point at a fixed distance, L_1, from the vessel. For non-holonomic vessels, this straight line to the look-ahead point cannot always be followed directly. Instead, the vessel follows a curved trajectory towards the look-ahead point, as illustrated in Figure 4.9.

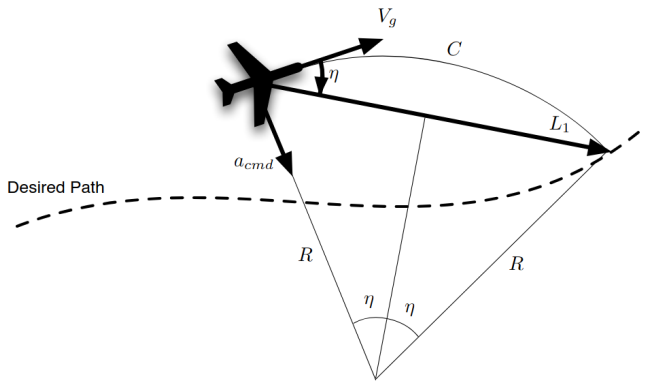

Figure 4.9: L_1 guidance law [23].

This guidance approach is extended for use in USVs, enabling them to follow the circular path towards the look-ahead point. A notable feature of L_1 and other guidance laws such as Line-of-Sight (LOS) guidance, is that as the vessel approaches the target trajectory, it becomes increasingly aligned with it. This behaviour is typically beneficial and results in accurate trajectory following.

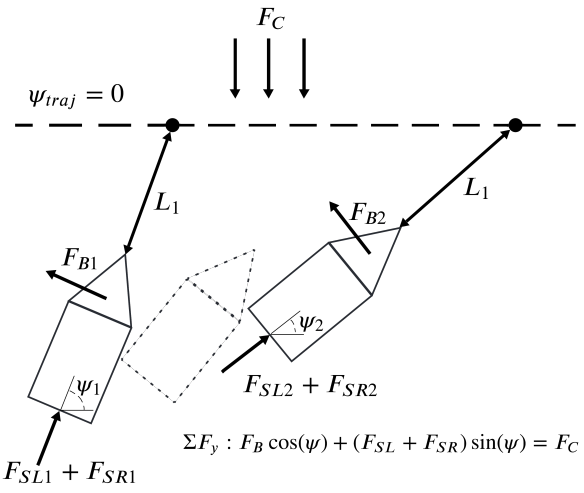

Figure 4.10: Free-body diagram of the USV at varying distances from the trajectory, under current disturbance. It is assumed that the USV is always aligned with the look-ahead point and that the trajectory is perfectly horizontal.

However, for underactuated USVs, significant disturbances, such as currents, introduce challenges. As shown in Figure 4.10, the effect of current on a USV approaching the trajectory can be visualised. Here,

F_{SL}, F_{SR}, and F_B indicate the thrust produced by the stern and bow thrusters, respectively. F_C indicates the force of currents acting on the vessel. Finally, ψ is the heading of the vessel, and L_1 is the look-ahead distance and is constant. For simplicity, it is assumed that the trajectory is perfectly horizontal and that the vessel is aligned with the look-ahead point, such that its trajectory towards the point is a straight line.

As the vessel approaches the trajectory, it becomes more parallel to it, reducing the effectiveness of the stern thrusters in pushing the vessel towards the line. Consequently, the bow thruster is required to compensate for the current force. However, the bow thruster may be insufficient to fully counteract the current, causing the vessel to drift away from the trajectory, rotate, and apply its stern thrusters.

An equilibrium angle is eventually reached, where the vessel is as close to the trajectory as possible while using maximum bow thrust. This equilibrium results in the constant offset observed in Chapter 2. Since the offset is a consequence of the guidance law, it is identical for both controllers, as observed from the simulation results presented in Chapter 2. Potential strategies to mitigate this offset, such as introducing a controller to shift the lookahead point away from the trajectory, are discussed in the appendix of Chapter 2.

4.4. ADRC Parameter Tuning

While the ADRC controller is generally robust to a wide variety of systems, disturbances, and uncertainties, the design of the controller itself is more sensitive. For an ADRC controller for a single control variable, there exist 9 parameters, an overview of which is provided in Table 4.1. The trajectory tracking controller design, as presented in Figure 4.1, employs three such controllers for surge velocity, lateral offset, and heading, resulting in a total of 27 parameters that must be tuned.

Parameter	For ADRC Component	Description
h_0	Tracking Differentiator	Filter factor
r_0	Tracking Differentiator	Tracking speed
h_1	NLSEF	Filter factor
r_1	NLSEF	Tracking speed
c	NLSEF	Damping factor
b_0	NLSEF	Control coefficient
β_{01}	Extended State Observer	1st order observer gain
β_{02}	Extended State Observer	2nd order observer gain
β_{03}	Extended State Observer	"Total disturbance" observer gain

Table 4.1: Parameters of a single ADRC controller.

This large number of parameters introduces complexity when initially tuning the controller. Although there are rules-of-thumb that can be translated from related control theory, such as observer gains derived from standard Luenberger observers, these were not always effective in practice. Observer gains, in particular, needed to be significantly reduced to avoid excessive sensitivity to noise in the measured vessel state. Although this adjustment did not hinder the performance of the ESO, it underscores the need to individually assess and evaluate all 27 parameters.

A sensitivity analysis, as presented in Section 4.2, can help identify local optimal parameter selections. However, performing this analysis for all 27 parameters is time-consuming. The structure of the simulation software stack, consisting of the Unity simulation environment and the digital twin of the control computer, complicates the implementation of parameter optimisation frameworks, such as Optuna. Although integration is possible, it would require significant development time, potentially exceeding the amount of time it would take to perform manual tuning.

Alternatively, a numerical simulation based on the manoeuvring model could facilitate the use of such tuning frameworks. This approach is simpler than integrating automatic tuning into the existing simulation stack. However, it would require the development and verification of a new numerical

simulation capable of replicating the control computer behaviour, as well as the effects of components such as GPS and IMU sensors, actuators, and control mixers. Consequently, this approach was not pursued in this thesis. The tuning of controller gains directly within the digital twin of the control computer also maximises the likelihood that the controller implementation would translate effectively to field tests.

Instead, manual tuning of the controllers was selected. This method provided the additional benefit of creating a thorough understanding of the effect of each parameter. This understanding is required for tuning during field tests, as manual adjustments are often necessary when parameters derived from simulation fail to perform as expected in real-world conditions.

From scientific literature, a significant portion of works on ADRC for USV control implement some form of self-tuning framework. Examples include the implementation of a firefly algorithm for online adjustment of controller parameters [14], as well as the use of a fuzzy controller to adjust ADRC parameters. Similar approaches, such as the application of particle swarm optimisation [18] and reinforcement learning [17], have also been proposed for the automatic adjustment of ADRC parameters.

The aforementioned frameworks have been validated in simulation, but not in physical vessels. Although these frameworks may theoretically improve performance and simplify the tuning process by reducing the reliance on precise parameter selection, their validity for physical vessels, particularly in industrial applications, remains uncertain. The added layer of abstraction introduced by these frameworks is likely to negatively impact the maintainability of deployed systems. For industrial applications, where robustness and ease of maintenance are prioritised, the feasibility of such frameworks must be critically evaluated. Future research should focus on bridging the gap between simulation-based validation and real-world applicability, ensuring that these self-tuning methods can reliably enhance performance without compromising system integrity.

5

Additional Field Testing Results and Discussion

This chapter presents additional findings from the field trials, expanding on the results discussed in Chapter 2 and providing further analysis of the ADRC framework's performance in real-world conditions. In particular, Section 5.1 investigates an undesirable response observed during cornering, where excessive heading corrections led to unintended velocity reductions. It is shown how this behaviour is caused by an excessive disturbance rejection, even in an environment where little external disturbances are present. A possible modification ADRC controller is shown, and its effect on tracking performance in simulation is evaluated.

5.1. Disturbance Rejection

During field trials, an undesirable behaviour was observed during cornering. Specifically, when the heading error became excessively large, the vessel responded by aggressively correcting the error, resulting in an overshoot. As part of the guidance law, this excessive heading correction also caused the velocity controller to reduce the vessel's surge velocity until the heading error decreased. This caused the vessel to stop at corners while aggressively adjusting its heading. The moment directly before this happens is marked as T_1, as shown in Figure 5.1, and it can be seen how this results in a significant deviation from the trajectory. This behaviour was also observed during sea trials in the same corner, but is more difficult to visualise in Figure 5.1.

The cause of this jerk becomes clear when evaluating the internal states of the controller. These states include the tracking errors e_1 and e_2 (state and derivative errors, respectively), as well as the disturbance estimate z_3. These states at T_1 are shown in Figure 5.2. From this, it is evident that the total disturbance estimate z_3, which accounts for both external disturbances and internal higher-order effects, exhibits a significant spike at this moment.

As z_3 is directly incorporated into the control law as a feedforward term, this results in a corresponding spike in torque demand. In the standard ADRC formulation, this feedforward term is not scaled by any coefficient and is directly combined with the control output [13]. As shown in these results, this leads to excessive "disturbance" rejection, despite the relatively low disturbance levels present during in-harbour trials. This suggests that z_3 in this instance primarily consists of internal uncertain effects rather than external disturbances.

5.1.1. Disturbance Rejection Scaling

To mitigate this excessive response, scaling the feedforward term z_3 by a coefficient γ could provide a more balanced control action. The topology of such a controller is shown in Figure 5.3.

This approach has been explored in previous works, where it is shown that the introduction of a scaling factor does not alter the estimated steady-state total disturbance in a reduced-order linear Extended State Observer (ESO) [24]. This proof can be extended to a nonlinear observer for a second-order system,

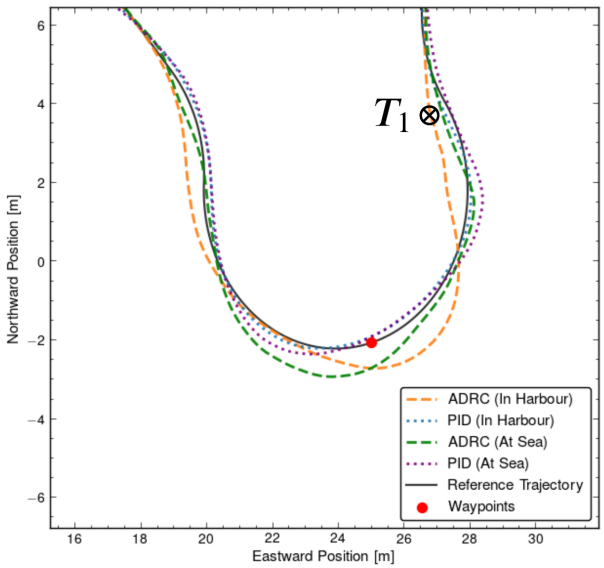

Figure 5.1: Trajectory at the moment T_1, after which the vessel exhibits a sudden jerk due to excessive heading corrections, during harbour trials.

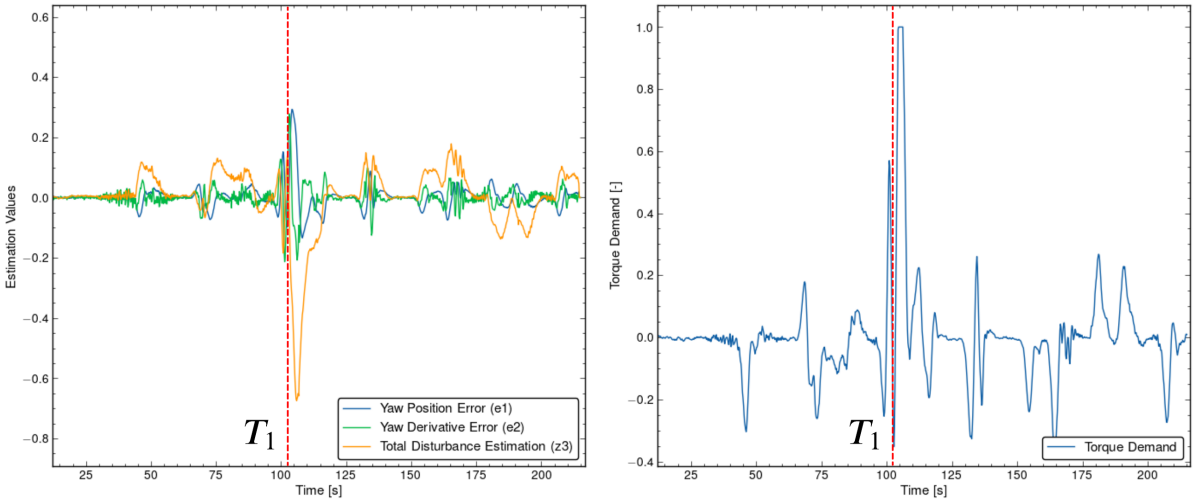

Figure 5.2: Internal states of the ADRC heading controller at T_1 during field trials, showing state errors e_1 and e_2, and the disturbance estimate z_3.

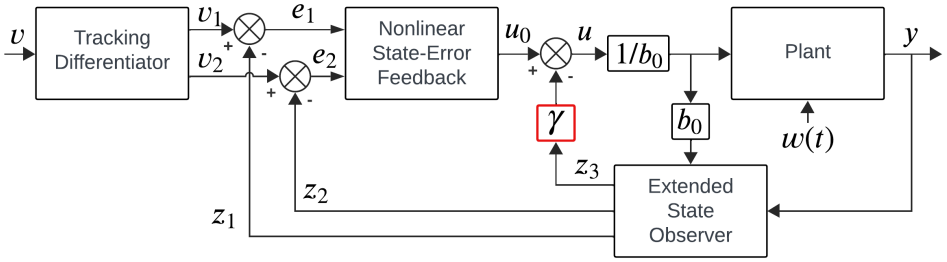

Figure 5.3: ADRC topology with an added total disturbance coefficient γ.

as demonstrated in Theorem 1.

Theorem 1. *The steady-state estimated total disturbance is independent of γ, and a non-linear state observer is not affected by γ.*

Proof: Consider the system (5.1) and the ESO (5.2):

$$\begin{cases} \dot{x}_1 = x_2 \\ \dot{x}_2 = x_3 + bu \\ \dot{x}_3 = G(t) \end{cases} \tag{5.1}$$

where $G(t) = \dot{F}(t)$ represents the derivative of the total disturbance $F(t)$. The ESO is formulated as:

$$\begin{cases} e = z_1 - y \\ \dot{z}_1 = z_2 - \beta_{01} e \\ \dot{z}_2 = z_3 + b_0 u - \beta_{02}\,\mathrm{fal}(e, \alpha_1, \delta) \\ \dot{z}_3 = -\beta_{03}\,\mathrm{fal}(e, \alpha_2, \delta) \end{cases} \tag{5.2}$$

These systems can be combined into a single error system, which is defined as follows:

$$\begin{cases} e = z_1 - y, \quad e_1 = z_1 - x_1, \quad e_2 = z_2 - x_2, \quad e_3 = z_3 - x_3 \\ \dot{e}_1 = e_2 - \beta_{01} e \\ \dot{e}_2 = e_3 + (b_0 - b)u - \beta_{02}\,\mathrm{fal}(e, \alpha_1, \delta) \\ \dot{e}_3 = -\beta_{03}\,\mathrm{fal}(e, \alpha_2, \delta) - G(t) \end{cases} \tag{5.3}$$

As the system has reached steady state, where $\dot{e}_1 = \dot{e}_2 = \dot{e}_3 = 0$, the error system can be simplified to:

$$e_3 = (b - b_0)u + \beta_{02}\,\mathrm{fal}(e, \alpha_1, \delta) \tag{5.4}$$

Recall that the ADRC control law using the scaling coefficient γ is defined as:

$$u = \frac{u_0 - \gamma z_3}{b_0} \tag{5.5}$$

Substituting (5.4) into (5.5) results in:

$$e_3 = \left(\frac{b}{b_0} - 1\right)(u_0 - \gamma z_3) + \beta_{02}\,\mathrm{fal}(e, \alpha_1, \delta) \tag{5.6}$$

At steady state, the system state is unchanging and therefore $\dot{x}_2 = 0$, meaning that:

$$x_3 + bu = 0$$

which implies:

$$z_3 - x_3 = z_3 + bu \tag{5.7}$$

Substituting (5.5) into (5.7) gives:

$$z_3 - x_3 = z_3 + \frac{b}{b_0}(u_0 - \gamma z_3) \tag{5.8}$$

Similarly, combining (5.4) and (5.7) results in:

$$z_3 - x_3 = \left(\frac{b}{b_0} - 1\right)(u_0 - \gamma z_3) + \beta_{02}\,\mathrm{fal}(e, \alpha_1, \delta) \tag{5.9}$$

By equating (5.8) and (5.9) and simplifying, we obtain:

$$u_0 = (\gamma - 1)z_3 + \beta_{02}\,\mathrm{fal}(e, \alpha_1, \delta) \tag{5.10}$$

Now, substituting (5.10) into (5.9) gives:

$$z_3 - x_3 = \left(1 - \frac{b}{b_0}\right) z_3 + \frac{b}{b_0}\beta_{02}\,\mathrm{fal}(e, \alpha_1, \delta) \tag{5.11}$$

which can be simplified to:

$$z_3 = \frac{b_0}{b}x_3 + \beta_{02}\,\mathrm{fal}(e, \alpha_1, \delta) \tag{5.12}$$

This shows that z_3 is independent of γ, given that e is also independent of γ. To show this, we again consider that for a steady-state response $\dot{e_3} = 0$:

$$\beta_{03}\,\mathrm{fal}(e, \alpha_2, \delta) = -G(t) \tag{5.13}$$

Since α_2, δ, and β_{03} are constants, and $G(t) = \dot{F}(t)$ describes the system dynamics (which do not depend on γ), it follows that e is independent of γ. Consequently, z_3 is also independent of γ.

5.1.2. Eliminating Steady-State Error

As demonstrated in the previous section, introducing the scaling coefficient γ does not affect the steady-state total disturbance estimation z_3. However, the addition of this scaling coefficient does lead to a steady-state error. This occurs because ADRC lacks an integral action, relying instead on the feed-forward term z_3 to compensate for steady-state errors in the total disturbance signal. These errors cannot be attributed to either the position error e_1 or the velocity error e_2. When $\gamma < 1$, the total disturbance is no longer fully counteracted, leading to tracking deviations [24].

A potential solution to mitigate this issue is to introduce an integral term within the Nonlinear Error State Feedback (NLSEF), modifying the control law as follows:

$$u = -\frac{\mathrm{fhan}(e_1, ce_2, r_1, h_1) + \gamma z_3}{b_0} + k_i \int_0^t e_1(\tau)d\tau \tag{5.14}$$

where the additional integral term aims to eliminate the remaining steady-state error.

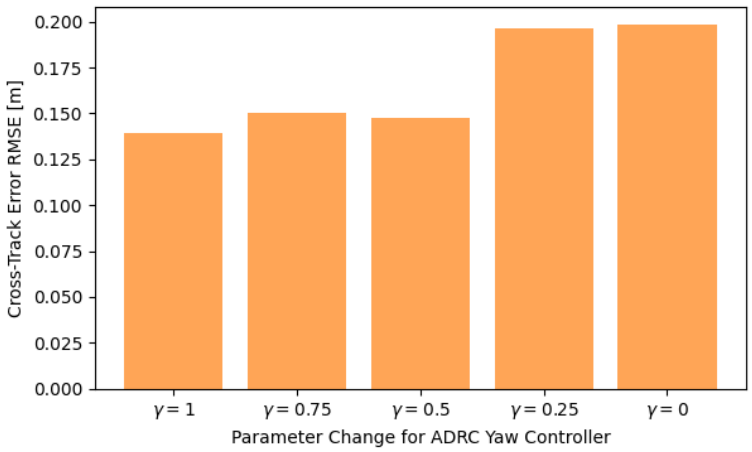

Figure 5.4: Effect of varying the scaling coefficient γ on simulated trajectory tracking in sea state 4. Each parameter setting is evaluated over a single trajectory.

A detailed analysis of this modified controller falls beyond the scope of this thesis. However, preliminary simulations have been conducted to assess the impact of coefficient γ on ADRC performance. The coefficient γ is changed for the heading controller, as this has the most significant effect on the cross-track error. To compensate for the steady-state error when $\gamma < 1$, an integral gain of $k_i = 0.1$ is applied. The vessel operates in a sea state 4 environment without additional wind or current disturbances. The results of these simulations are presented in Figure 5.4.

It is important to note that the behaviour observed in field trials, as shown in Figure 5.1, could not be accurately reproduced in simulation. This discrepancy is likely attributable to limitations in the wave disturbance model, which does not fully capture the momentum transfer from waves to the vessel. Consequently, simulated disturbances may be less pronounced than those encountered under real-world conditions. Alternatively, the DWP2 package primarily simulates second-order effects, whereas, in reality, the estimated total disturbance z_3 includes higher-order effects that are not adequately represented in the simulation.

Nevertheless, Figure 5.4 reveals a clear trend: reducing γ leads to an increase in XTE, confirming that reduced feed-forward compensation negatively affects tracking accuracy. Future research should focus on evaluating such a modified controller in sea trials to identify an optimal trade-off. Specifically, a balance must be found where γ is reduced enough to prevent the unwanted behaviour seen in Figure 5.2 while still maintaining acceptable tracking performance.

6

Conclusion

This thesis investigates the application of Active Disturbance Rejection Control (ADRC) for trajectory tracking of an Unmanned Surface Vessel (USV) in near-shore conditions. While ADRC has been repeatedly validated in simulation in prior research [14]–[19], no studies have previously evaluated its performance on a seagoing USV. Through the development of a realistic simulation framework and field trials in Scheveningen, ADRC was compared to a baseline PID controller, assessing its effectiveness in mitigating the effects of environmental disturbances such as waves, currents, and wind. The research aimed to answer the following question: **How does the performance of a second-order ADRC strategy for trajectory tracking compare to a PID controller when evaluated through simulation and field experiments?**

The results demonstrate that ADRC consistently outperforms PID in reducing cross-track error by 30–40% in simulation and by 10–20% in field trials. The extent of this improvement was less pronounced in field trials than in simulations, primarily due to a difference in the turning radius between the simulated and field experiments. This difference makes it difficult to directly compare the simulation and field results. Further simulation studies using identical reference paths should enable quantitative comparison between simulation and field-testing results.

A key limitation of the ADRC framework identified in this thesis is its increased energy consumption compared to the baseline PID controller. In simulation, this increase was observed only in the absence of current; with current present, ADRC completed the trajectory faster, resulting in equal battery usage. In field trials, the transition from harbour to near-shore conditions led to a substantial increase in energy consumption, with ADRC requiring approximately 50% more control effort than PID. These findings suggest that while ADRC improves trajectory tracking, its higher energy demand may limit its practicality for commercial USV applications, where endurance is a primary concern.

This increased energy demand is partly due to an excessively high feed-forward disturbance rejection term. A proposed modification demonstrated that this change does not affect the state observer's total disturbance estimation but increases cross-track error in simulation. Since the overly aggressive response seen in field trials was not replicated in simulation, its impact on efficiency remains unclear. More sea trials are needed to assess whether this trade-off is justified. Another research direction to improve ADRC efficiency is incorporating model information into the state observer, which could reduce excessive control effort by distinguishing internal dynamics from external disturbances.

In general, the findings confirm the potential of ADRC as a robust control framework for USV trajectory tracking. However, its applicability to commercial, seagoing USVs requires significant improvements in efficiency. For small electric vessels such as the DUS V2500, the increase in energy consumption imposes a major limitation, as it directly affects the endurance of the vessel. Although the advantages offered by ADRC are evident, further modifications to the standard framework are required to achieve a trade-off between performance and efficiency in practical applications.

References

[1] J. Yuh, G. Marani, and D. Blidberg, "Applications of marine robotic vehicles," *Intelligent Service Robotics*, vol. 4, pp. 221–231, Oct. 2011. DOI: 10.1007/s11370-011-0096-5.

[2] J. H. Stel, "Exploring and exploiting deep ocean space," in *Ocean Literacy: Understanding the Ocean*, K. C. Koutsopoulos and J. H. Stel, Eds. Cham: Springer International Publishing, 2021, pp. 65–92, ISBN: 978-3-030-70155-0. DOI: 10.1007/978-3-030-70155-0_4.

[3] Z. Liu, Y. Zhang, X. Yu, and C. Yuan, "Unmanned surface vehicles: An overview of developments and challenges," *Annual Reviews in Control*, vol. 41, pp. 71–93, 2016, ISSN: 1367-5788. DOI: 10.1016/j.arcontrol.2016.04.018.

[4] V. Bolbot, A. Sandru, T. Saarniniemi, O. Puolakka, P. Kujala, and O. A. Valdez Banda, "Small unmanned surface vessels—a review and critical analysis of relations to safety and safety assurance of larger autonomous ships," *Journal of Marine Science and Engineering*, vol. 11, no. 12, 2023, ISSN: 2077-1312. DOI: 10.3390/jmse11122387.

[5] G. Roberts and R. Sutton, *Advances in Unmanned Marine Vehicles*. Advances in Unmanned Marine Vehicles, Jan. 2006, pp. 1–442, ISBN: 978-0-86341-450-3. DOI: 10.1049/PBCE069E.

[6] *How USVs can Change the Offshore Inspection Market Through Novel Operating Models*, vol. Day 1 Mon, May 06, 2024, OTC Offshore Technology Conference, May 2024, D011S003R003. DOI: 10.4043/35258-MS.

[7] J. Bosboom and M. Stive, *Coastal Dynamics*. TU Delft OPEN Publishing, 2021, ISBN: 978-94-6366-370-0. DOI: 10.5074/T.2021.001.

[8] A.-A. Al-Habashneh, C. Moloney, and E. Gill, "Ocean wave spectrum estimation from marine radar data using the polar Fourier transform," in *OCEANS 2014 - TAIPEI*, 2014, pp. 1–6. DOI: 10.1109/OCEANS-TAIPEI.2014.6964484.

[9] H. Xu and C. Guedes Soares, "Review of path-following control systems for maritime autonomous surface ships," *Journal of Marine Science and Application*, vol. 22, pp. 153–171, Jul. 2023. DOI: 10.1007/s11804-023-00338-6.

[10] L. C. McNinch, H. Ashrafiuon, and K. R. Muske, "Optimal specification of sliding mode control parameters for unmanned surface vessel systems," in *2009 American Control Conference*, 2009, pp. 2350–2355. DOI: 10.1109/ACC.2009.5160064.

[11] E. Børhaug, A. Pavlov, E. Panteley, and K. Y. Pettersen, "Straight line path following for formations of underactuated marine surface vessels," *IEEE Transactions on Control Systems Technology*, vol. 19, no. 3, pp. 493–506, 2011. DOI: 10.1109/TCST.2010.2050889.

[12] T. I. Fossen, M. Breivik, and R. Skjetne, "Line-of-sight path following of underactuated marine craft," *IFAC Proceedings Volumes*, vol. 36, no. 21, pp. 211–216, 2003, 6th IFAC Conference on Manoeuvring and Control of Marine Craft (MCMC 2003), Girona, Spain, 17-19 September, 1997, ISSN: 1474-6670. DOI: 10.1016/S1474-6670(17)37809-6.

[13] J. Han, "From PID to active disturbance rejection control," *IEEE Transactions on Industrial Electronics*, vol. 56, no. 3, pp. 900–906, 2009. DOI: 10.1109/TIE.2008.2011621.

[14] J. Hu, Y. Ge, X. Zhou, S. Liu, and J. Wu, "Research on the course control of USV based on improved ADRC," *Systems Science & Control Engineering*, vol. 9, no. 1, pp. 44–51, 2021. DOI: 10.1080/21642583.2020.1865216.

[15] F. Chen, H. Xiong, and J. Fu, "The control and simulation for the ADRC of USV," in *2015 Chinese Automation Congress (CAC)*, 2015, pp. 416–421. DOI: 10.1109/CAC.2015.7382536.

[16] Y. Fan, L. Liu, and Y. Yang, "ADRC course control for USV based on fuzzy self-tuning," in *2021 4th International Conference on Intelligent Autonomous Systems (ICoIAS)*, 2021, pp. 307–311. DOI: 10.1109/ICoIAS53694.2021.00061.

[17] Y. Zheng, J. Tao, Q. Sun, *et al.*, "Soft actor–critic based active disturbance rejection path following control for unmanned surface vessel under wind and wave disturbances," *Ocean Engineering*, vol. 247, p. 110 631, 2022, ISSN: 0029-8018. DOI: 10.1016/j.oceaneng.2022.110631.

[18] M. Fu, Q. Wang, Y. Wang, and Y. Xu, "Design of ADRC for unmanned surface vehicle heading based on immune particle swarm optimization," in *2021 IEEE International Conference on Mechatronics and Automation (ICMA)*, 2021, pp. 130–135. DOI: 10.1109/ICMA52036.2021.9512588.

[19] H. Li, H. Chen, N. Gao, N. Aït-Ahmed, J.-F. Charpentier, and M. Benbouzid, "Ship dynamic positioning control based on active disturbance rejection control," *Journal of Marine Science and Engineering*, vol. 10, no. 7, 2022, ISSN: 2077-1312. DOI: 10.3390/jmse10070865.

[20] D. Wu, K. Yuan, Y. Huang, Z.-M. Yuan, and L. Hua, "Design and test of an improved active disturbance rejection control system for water sampling unmanned surface vehicle," *Ocean Engineering*, vol. 245, p. 110 367, 2022, ISSN: 0029-8018. DOI: https://doi.org/10.1016/j.oceaneng.2021.110367.

[21] S. F. Hoerner, *Fluid-Dynamic Drag: Practical Information on Aerodynamic Drag and Hydrodynamic Resistance*, 2nd ed. 1965, pp. 3–17.

[22] F. Alfahmi, S. Hakim, R. Dewi, and A. Khaerima, "Utilization of data mining classification techniques to identify the effect of madden-julian oscillation on increasing sea wave height over east Java waters," *IOP Conference Series: Earth and Environmental Science*, vol. 399, p. 012 062, Dec. 2019. DOI: 10.1088/1755-1315/399/1/012062.

[23] R. Curry, M. Lizarraga, B. Mairs, and G. H. Elkaim, "L+2, an improved line of sight guidance law for UAVs," in *2013 American Control Conference*, 2013, pp. 1–6. DOI: 10.1109/ACC.2013.6579804.

[24] J. Zou, "Robust active disturbance rejection control scheme for quadrotor UAVs: Experimental prototyping," English, Master's Thesis, Eindhoven University of Technology, Aug. 2018.